

American Journal of Science

JUNE 2010

MODELING METAMORPHISM IN COLLISIONAL OROGENS INTRUDED BY MAGMAS: I. THERMAL EVOLUTION

T. LYUBETSKAYA and J. J. AGUE

Department of Geology and Geophysics, Yale University, P.O. Box 208109, New Haven, Connecticut 06520-8109, USA; jay.ague@yale.edu

ABSTRACT. This paper presents the results of two-dimensional (2-D) numerical modeling that reconstructs the thermal evolution and the flow of fluid in a collisional overthrust setting with syn-metamorphic magmatism. The goal of the study is to explore the relationships between regional metamorphism and magmatic activity. Our results demonstrate the strong effects that syn-metamorphic magmatism exerts on the thermal structure of the thickened crust. Magmatic intrusions in the form of repetitive sills of mafic or intermediate-felsic compositions introduced at different levels in the thickened crust section may produce Buchan and Barrovian-type metamorphic sequences, as well as rocks in the granulite facies of metamorphism. The peak temperatures in crustal rocks around intrusions are increased by more than 100 °C from their values for the non-magmatic case; the timescales of peak temperature attainment in rocks at short distances from the intrusions are only 1 Myr or less. The peak temperature attainment is synchronous within the different metamorphic zones over the depth range of up to 20 km. These features differ strongly from those in the overthrust model without magmatism, characterized by broad thermal peaks spanning 5 to 10 Myr and non-synchronous attainment of peak conditions for rocks at different depths, with ~5 Myr delay for every 10 km of depth (exhumation rate = 1 mm yr⁻¹). The specific peak metamorphic mineral assemblages that develop in model rock of metapelitic composition as a result of magmatism are largely controlled by the depth of magma emplacement: intrusion into the lower plate of the overthrust zone leads to the development of amphibolite facies mineral assemblages in the staurolite, kyanite and garnet-biotite (without chlorite) zones, as well as considerable volumes of granulite facies rocks. Emplacement of intrusions at mid-crustal depths of 15 to 35 km produces minerals of low-pressure/high-temperature (LP/HT) metamorphic zones, such as cordierite-biotite-K-feldspar, in addition to staurolite, kyanite, and sillimanite zones. When mid-crustal magmatism is initiated at earlier times in the model thrust exhumation history, the LP/HT metamorphic zones may not be preserved in the crustal section due to surface erosion. All of the models predict extremely steep, approximately isobaric Metamorphic Field Temperature Gradients (MFTGs) around the edges of the intrusions and along the contacts of thick isolated sills. In some cases, the transition from chlorite to sillimanite zones of metamorphism at the side of the magmatic region may take place in less than 1 km. The magmatism-related MFTGs stand in contrast to the regional metamorphic gradients produced by crustal thickening that form at the flanks of the overthrust zone distal to the magmas. Here, the transition from the chlorite zone to high-grade mineral assemblages takes place over 20 to 40 km, and the pressure of peak temperature attainment increases by as much as 0.3 GPa from low to high grade.

INTRODUCTION

Strong spatial and temporal associations between regional metamorphism and magmatic activity have been observed in many orogenic belts, including the type locality of Barrovian metamorphism in Scotland (Barrow, 1893; Miyashiro, 1973). Such

observations have led to intensive discussions regarding the genetic links between regional metamorphism and magmatism. In particular, the role of magmatism in the global heat budget of regional metamorphism has been debated in the literature (for example, Wickham and Oxhburgh, 1985; Lux and others, 1986). Several numerical models indicate that the highest-temperature parts of Barrovian sequences observed in collisional orogens could have formed only if additional sources of heat beyond the thermal relaxation of overthickened crust were available during regional metamorphism (Huerta and others, 1996; Jamieson and others, 1998). The requirements for strong heat sources operating at mid-crustal and upper-crustal levels are even more severe in models that try to simulate Buchan-type low-pressure, high-temperature (LP/HT) metamorphic conditions (De Yoreo and others, 1991, and references therein). The common presence of igneous rocks in areas of high-temperature regional metamorphism suggests that the heat required for the development of high metamorphic temperatures in many tectonic settings may, at least in part, be provided by magmatism (for example, Yardley and others, 1987; Hanson and Barton, 1989; Barton and Hanson, 1989; Sisson and others, 1989; Baxter and others, 2002; Ague and Baxter, 2007; Lancaster and others, 2008; Dutrow and others, 2010).

In this work and in the accompanying paper (referred to herein as Part II) we present the results of two-dimensional (2-D) forward numerical modeling that reconstructs the thermal evolution and the evolution of fluid flow during regional metamorphism accompanied by syn-metamorphic magmatism. Our models combine the most important features of purely thermal numerical simulations of crustal-scale magmatism (for example, Lux and others, 1986; Annen and others, 2006) with a 2-D representation of regional fluid flow during metamorphism in an overthrust setting (compare Hanson, 1997; Lyubetskaya and Ague, 2009a). The forward modeling approach allows us to systematically explore the relationships between major characteristics of syn-metamorphic magmatism—including the timing, depths, temperatures and rates of magma emplacement—and the P-T-conditions of regional metamorphism. We summarize this information in the form of schematic crustal cross-sections that depict the spatial distribution as well as the temporal evolution of prograde metamorphic mineral assemblages attained by crustal rocks having a representative aluminous pelitic composition.

In Part II of this work we explore patterns of fluid flow that may arise in an overthrust setting in the presence of magmatic intrusions. Furthermore, we assess the effects that partial melting of wall rocks, metamorphic reactions, and the flow of fluid may have on the thermal history of crustal rocks. Finally, we integrate the results of Parts I and II in order to explore the implications of our model results for the origin and evolution of the Barrovian and Buchan metamorphic zones in Scotland.

As described below, our treatment of magmatism and fluid flow incorporates many important simplifications. However, advancements in geological understanding as well as numerical modeling are often not possible without careful and accurate testing of relatively simple models, which investigate the possible effects of prescribed parameters without including explicit representation of many of the processes controlling those parameters. We emphasize that our models do not presume to reproduce all the complex geological processes that occur during regional metamorphism, and are not intended to “mimic” any specific metamorphic belt. They were instead designed to test hypotheses about the impact of magmatism on regional metamorphism, and to make testable predictions regarding metamorphic evolution in systems intruded by magmas. Our intention is to delineate a large part of the space of possible model solutions for realistic ranges of the most basic parameters characterizing coupled magmatism and metamorphism. This, in turn, allows us to construct hypothetical thermal evolutions for metamorphic terranes with magmatism that should provide

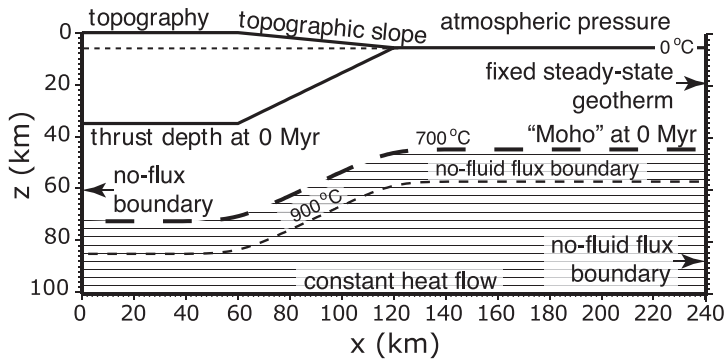


Fig. 1. Model geometry illustrating some important initial and boundary conditions. Surface held at atmospheric pressure and 0°C for all model times. Model "Moho" is defined by the 700°C isotherm. Below this depth, rocks contain no structural water bound in hydrous minerals (horizontal ruled area). There are no fluid fluxes across the boundaries at $x = 0$ km and $x = 240$ km, or across the 900°C isotherm. No heat fluxes are allowed across the boundary at $x = 0$ km; the boundary at $x = 240$ km has T fixed by the steady-state geotherm. Constant mantle heat flux ($35 \cdot 10^{-3} \text{ W m}^{-2}$) prescribed at $z = 100$ km. See text and Appendix for further discussion.

some general guidelines for interpreting field data from such geological settings. In addition, these simple models may turn out to be useful benchmarks for analyzing future, more complex (and possibly, inverse) models of metamorphism and magmatism in specific geological localities.

MODEL FORMULATION

With the forward modeling approach used herein it would be intractable to encompass all the possible variations and mutual dependences of the many parameters related to crustal thermal structure and fluid flow during regional metamorphism and magmatism. We therefore take into account the first-order variability at crustal conditions of those parameters that directly influence the large-scale behavior of our models, including the depth dependency of radiogenic heat production through the crust, and the dependence of fluid density on P-T conditions. However, we consciously ignore variations in many other parameters, such as rock density and thermal diffusivity, heat capacities of rock and fluid, and the latent heat of fusion. For such parameters we use constant values throughout the model crust (see Appendix and table A1). Recent studies, including Gerya and others (2002) and Whittington and others (2009), have shown that variations in some of these parameters may affect the temperatures and time scales of crustal thermal evolution to varying degrees. While these effects could certainly be important in some geologic settings, we concentrate instead on juxtaposing and comparing relatively simple models in an attempt to test first-order hypotheses bearing on the relationships between regional metamorphism and magmatism. Our approach is that the thermal effects produced by changes in the most basic features of magmatism, including the rates, temperatures and depths of magma emplacement as well as the dimensions of individual intrusions, are likely to dominate thermal evolution.

The numerical modeling is similar to that described by Lyubetskaya and Ague (2009a). We solve a system of partial differential equations that include energy conservation, mass conservation and Darcy's law (momentum conservation) for compressible H_2O fluid. The list of the equations and the details of the model formulation are provided in the Appendix. The vertical dimension of the model is 100 km, and the horizontal dimension is 240 km (fig. 1). The overthrust geometry is represented with a

thrust sheet of an average crustal thickness (35 km) that has been emplaced over the distance of 120 km from the left boundary, the upper 5 km elevated above the surface comprising the topography. We do not examine thrust sheets of different initial thicknesses; however, some models simulate magmatism that begins after considerable exhumation and thinning of the upper plate has occurred.

The emplaced crustal section tapers off between 60 km and 120 km from the left boundary. Local erosion rates are assumed to be in balance with rock uplift rates at the surface so that the topography is in steady-state and is not leveled with exhumation (Willett and Brandon, 2002). The exhumation rate is held constant for $x = 0$ –60 km under the region of highest model elevation, and then decreases linearly to zero from $x = 60$ to $x = 120$ km.

The equations are solved using the finite difference method and a grid spacing of 0.5 km in the z dimension and 2 km in the x dimension. In some models a finer grid size is used (0.5 km in z and 1 km in x). The time step in most of the simulations is 5,000 years for energy conservation and 20,000 years for mass and momentum conservation equations. The greater time step for mass and momentum conservation expedites the numerical calculations as the iterative solution search for fluid pressure is the most time-consuming stage of the computations; the choice is also compatible with the general rates of pressure evolution in the system.

The total simulation time for each model is determined by the time required for eroding away the upper plate of the thrust (maximum thickness 35 km) in the doubled crust segment of the model. For the exhumation rates considered in this work—1.5 mm yr⁻¹, 1 mm yr⁻¹ and 0.5 mm yr⁻¹—the simulation times are correspondingly 24 Myr, 35 Myr and 70 Myr. These rates are broadly comparable to those estimated for a number of localities worldwide including the European Alps (0.4–0.7 mm yr⁻¹; Bernet and others, 2001), Denali (~1 mm yr⁻¹; Fitzgerald and others, 1993), the Cordillera Real of the Bolivian Andes (≤0.6 mm yr⁻¹; Safran and others, 2006), the central massif of the Olympic Mountains (0.75 mm yr⁻¹; Brandon and others, 1998), and the Nanga Parbat region (~3 mm yr⁻¹; Moore and England, 2001). They are slower than observed in some rapidly-exhuming orogens, such as Taiwan (see Willett and others, 2003), but the range of rates investigated is sufficient to illuminate several important relationships between exhumation, magmatism, and metamorphism. Some implications for faster exhumation at 5 mm yr⁻¹ are considered in Part II.

The initial thermal structure of the model crustal section is calculated based on a steady-state crustal geotherm with representative values of radiogenic heat production and basal heating (Appendix; table A1). In the thrust region, the superposition of two steady-state geotherms results in an initial sawtooth thermal profile. As the sawtooth geotherm may imply unrealistically fast convergence rates (Shi and Wang, 1987), we allow it to relax conductively for 0.5 Myr before the simulations start (see fig. 1 in Lyubetskaya and Ague, 2009a).

Our approach to modeling deep and mid-crustal magmatism employs the concept of the crustal “hot zone” proposed by Annen and Sparks (2002) and Annen and others (2006). Magmatic intrusions (predominantly mafic) are modeled as successions of horizontal sills that are emplaced instantaneously at different levels within the thickened crust region which, in our examples, has an aluminous metapelitic composition. The amount of mafic magma intruded in our simulations (default model = 5 km total thickness) is much less than that considered by Annen and others (2006; >15 km). Annen and others (2006) modeled the large inputs of heat and mass needed to generate intermediate and silicic arc magmas in crustal hot zone environments. Our focus, however, is on regional metamorphism, so we have scaled back the amount of igneous intrusion so as not to produce the large-scale crustal melting characteristic of arcs.

The mafic magmas could be derived from a number of sources, including partial melting of the mantle wedge above subduction zones triggered by addition of volatiles or melts from the subducted slab (Annen and others, 2006, and references therein); decompression melting resulting from asthenospheric upwelling through slab windows that form during subduction of ridge systems (Gorring and Kay, 2001); or decompression melting during extensional tectonism. A detailed discussion of these and other magmatic scenarios is beyond the scope of this paper. We note, however, that emerging evidence suggests that the addition of heat and mass to the crust, largely in the form of mafic magmas, can be significant during mountain building. One likely example is the Acadian orogen in northern New England (Dorais, 2003). Furthermore, it is clear that considerable volumes of syn-orogenic, mantle-derived mafic magma can intrude regional metamorphic sequences in regions of crustal thickening, as is the case for the classic Barrovian and Buchan zones of Scotland (Baxter and others, 2002; Oliver and others, 2008, and references therein). These metamorphic rocks are thought to have overlain a subducting slab that possibly fragmented to produce a slab window (Oliver and others, 2008), but much work remains to gain a full understanding of magma petrogenesis. Syn-orogenic, arc-related magmatism in the Irish Dalradian (Friedrich and others, 1999) may have supplied much of the heat for peak amphibolite facies metamorphism in Connemara (Yardley and others, 1987; Reverdatto and Polyansky, 2004).

The monitoring of the temperature evolution of each intrusion starts 5,000 yrs (that is, single time-step) after magma emplacement. Because of the relatively sparse numerical grid in our models and the thinness of the intrusions (1 or 2 grid cells), convection of magma within the sills is neglected. For thicker sills with large lateral extent this simplification is likely to slightly underestimate the heat flow from the intrusions, and slightly overestimate cooling times. Other types of intrusions, such as diapirs or lopoliths, are not considered. We note, however, that our models with 10 or 20 sills that are closely spaced within the depth interval of only 15 or 20 km may to some extent approximate the emplacement of a magmatic diapir (fig. 2B, D). Because magmas generally ascend significantly faster than they cool (Marsh, 1982; Mahon and others, 1988), the emplacement temperatures are modeled at about the liquidus level for basaltic (1200 °C) and intermediate felsic (850 °C) magmas.

The default model of syn-metamorphic magmatism in our work includes ten individual sills with a thickness of 500 m emplaced randomly within the depth range of 15 to 35 km (“mid-crustal intrusion”) or 35 to 50 km (“deep intrusion”). The total thickness of intruded sills in this type of model is thus 5 km. The lateral dimension of each sill varies in a random way between 10 and 50 km. The timing of the magmatism is 0, 5 or 15 Myr after the start of the simulation; the sills are emplaced either: a) every 20,000 years (“fast intrusion” at a rate of 2.5 cm yr⁻¹) or b) every 200,000 years (“slow intrusion” at a rate of 0.25 cm yr⁻¹). The above volumes and rates of magma emplacement are representative of magma productivity estimates during intracontinental volcanism and plutonism (for example, Crisp, 1984) and are in the parameter range explored by Annen and others (2006). In addition to this default configuration, we present a number of simulations in which the thickness and lateral dimensions of individual sills, the rate of emplacement, and the timing of intrusion were varied systematically (see table 1 for the list of simulations).

We consider two different mechanisms of magma emplacement within crustal rocks (fig. 2). The first mechanism assumes the volume-for-volume replacement of wall rock by magma (fig. 2A, B). In the second scenario, the newly emplaced magma is accommodated by vertical downward displacement of the rock column that underlies the intrusion. Such vertical movement leads to crustal thickening as a result of magmatic intrusion. This scenario is employed in a 1-D model of magmatism by Annen

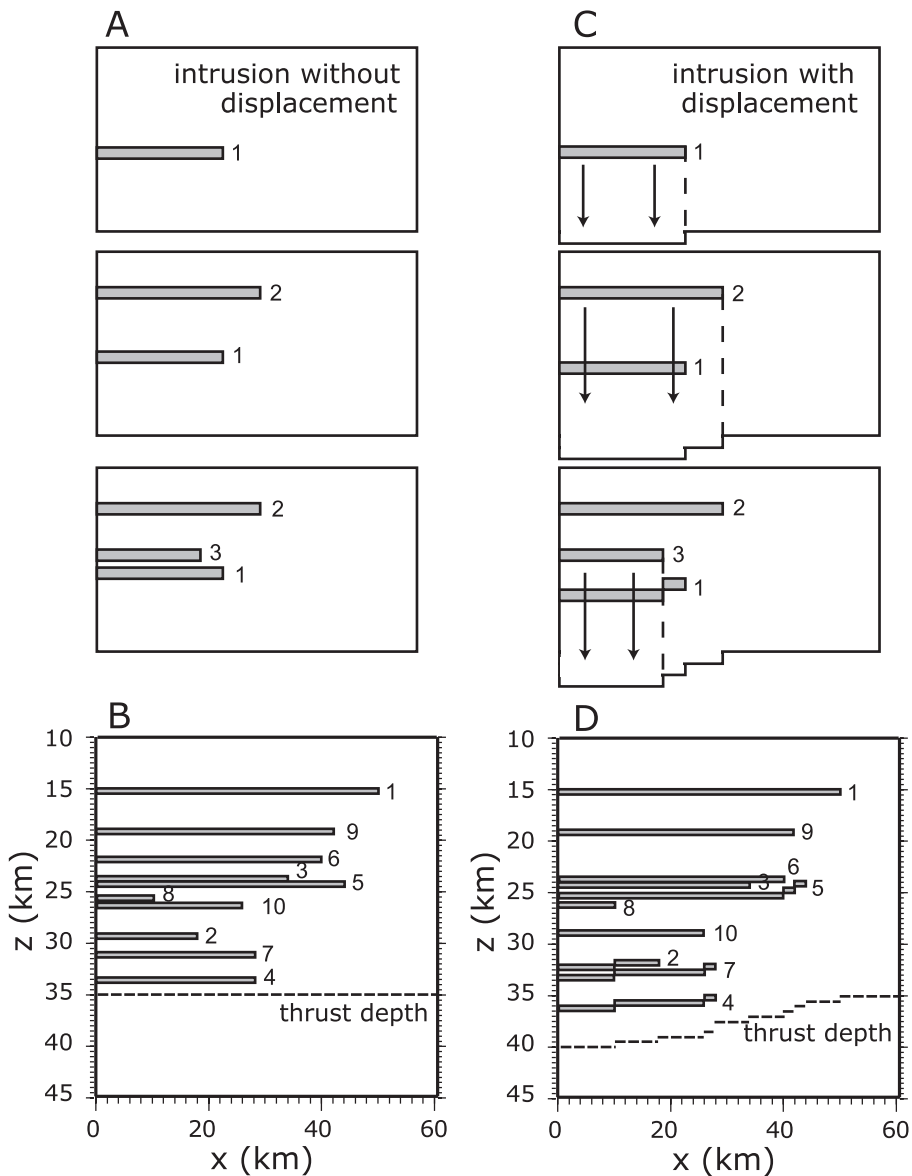


Fig. 2. (A) Schematic diagram illustrating the positioning of consecutive sill intrusions in a model without wall rock displacement. (B) Location of ten sills in the default configuration of depth and lateral dimensions, for a model with mid-crustal magmatism initiated at 0 Myr, fast intrusion rate, and no wall rock displacement. (C) Schematic diagram illustrating the positioning of consecutive sill intrusions in a model with downward wall rock displacement. (D) Location of ten sills in the default configuration of depth and lateral dimensions, for a model with mid-crustal magmatism initiated at 0 Myr, fast intrusion rate, and downward wall rock displacement.

and others (2006). In our models with 2-D geometry, the downward rock displacement may also produce inflexions in the sills partly located within the moving rock column (fig. 2C, D). In nature, magma intrusion would probably be accommodated by some combination of vertical and lateral deformation or displacement of the wall rock as

TABLE 1
Variations of model parameters explored in numerical experiments

| Number of sills and total thickness of intrusions | Rates of emplacement | Depth range of emplacement | Time of emplacement | Parameter variations |
|---|---|---|--|--|
| 10 sills 0.5 km thick; 5 km (default) | 0.25 cm yr ⁻¹ ("slow") 0.5 cm yr ⁻¹ 1.0 cm yr ⁻¹ 2.5 cm yr ⁻¹ ("fast") | 15-35 km ("mid-crustal") 35-50 km ("deep") | 0 Myr 3.33 Myr 5 Myr 10 Myr 15 Myr | Magma intrusion with / without wall rock displacement (Parts I, II) Erosion rates 0.5, 1.0, 1.5, 5.0 mm yr ⁻¹ (Parts I, II) Sill lateral dimensions 10-50 km or 6-10 km (Part I) Emplacement temperature 1200°C or 850°C (Part I) Retrograde reaction present / absent (Part II) Reaction enthalpy >0, >0, or =0 (Part II) Fusion enthalpy >0 or =0 (Part II) Basal heating below the thrust: 35, 70, or 105 mW m ⁻² (Part II) Different random configurations of individual sill depth and dimensions (not shown) Fluid exsolution from magmas/fluid consumption by crustal melts (discussed in Part II) |
| 3 sills 1 km thick; 3 km | | | | |
| 6 sills 0.5 km thick; 3 km | | | | |
| 6 sills 1 km thick; 6 km | | | | |
| 5 sills 2 km thick; 10 km | | | | |
| 10 sills 1 km thick; 10 km | | | | |
| 20 sills 0.5 km thick; 10 km | | | | |

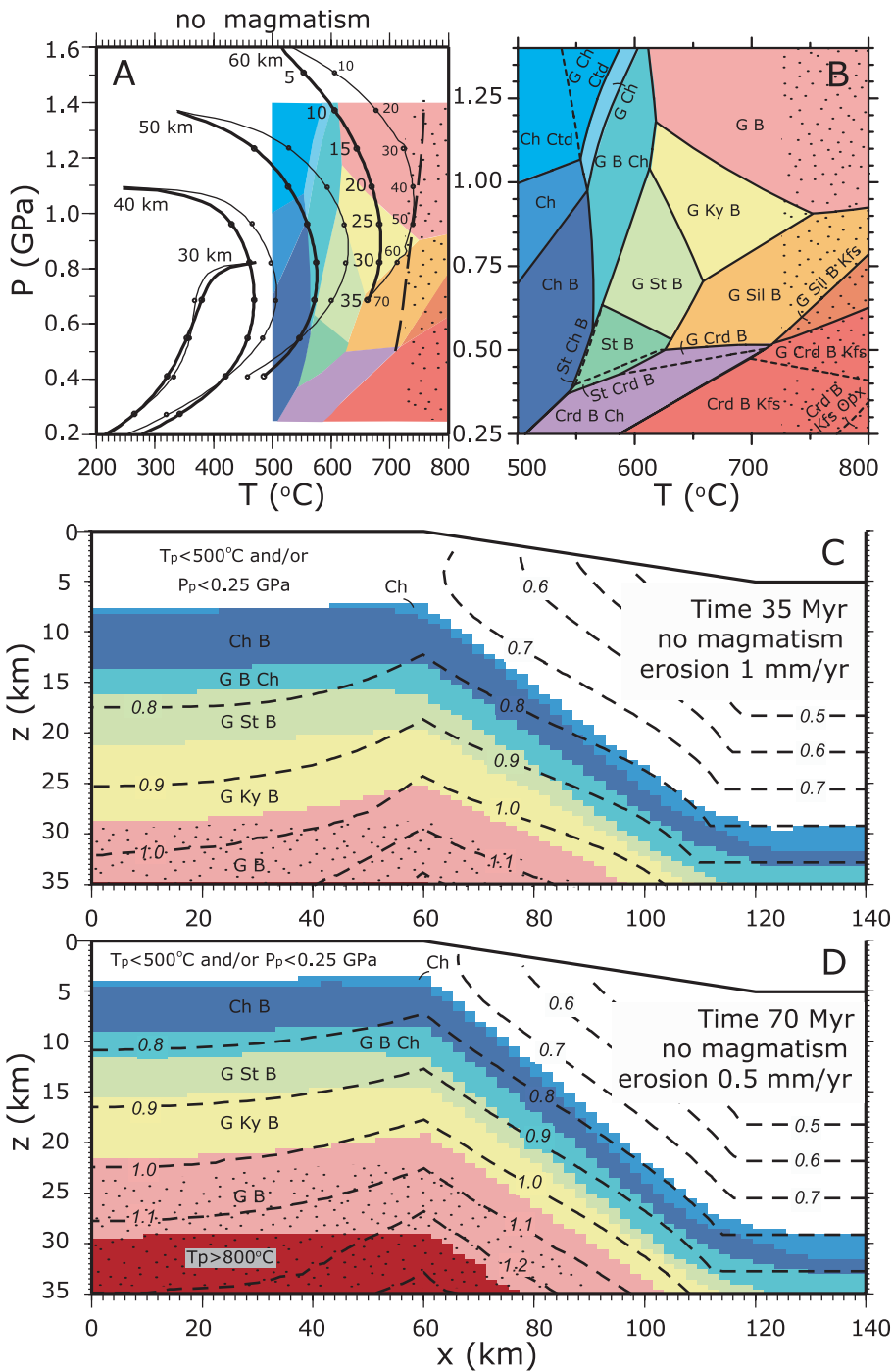


Fig. 3.

well as by some amount of wall rock melting and replacement. The two scenarios therefore present end-members highlighting different aspects of the complicated “room problem” of igneous petrology. Our default models assume the intrusion of magmatic sills with downward displacement (fig. 2C, D). Some of the default model results will then be contrasted with models that assume magma intrusion without displacement.

We use constant values for thermal conductivity, heat capacities of rock and fluid and latent heats of fusion/crystallization for metapelitic and igneous rock (table A1). The variations of melt fraction with temperature for the crustal wall rock of metapelitic composition, as well as for magmatic sills of basaltic and intermediate-felsic compositions are from Annen and Sparks (2002) and Annen and others (2006). Model crustal partial melts do not migrate away from their source rocks. Although this treatment is clearly a simplification, it is appropriate for some scenarios, including *in situ* migmatite genesis. We account for the latent heat of fusion of the wall rocks during heating, as well as the latent heat of crystallization during cooling. No partial melting of rocks below the model “Moho” (fig. 1) is considered.

The model crustal section is assumed to comprise aluminous metapelitic rocks. Pseudosection calculations to compute the P-T stability fields of metamorphic mineral assemblages for a representative bulk composition in the system K_2O -FeO-MgO- Al_2O_3 - SiO_2 - H_2O (Powell and others, 1998; fig. 3B) were done using Theriak Domino (version 150508; <http://titan.minpet.unibas.ch/minpet/theriak/theruser.html>; de Capitani and Brown, 1987; de Capitani, 1994). The default thermodynamic data and activity models were used, except the standard enthalpy of formation of Mg-staurolite was modified slightly as described by Bucholz and Ague (2009). All mineral assemblages coexist with quartz and water. Most assemblages also coexist with muscovite, except for the very highest temperature rocks in which muscovite has broken down to form K-feldspar. The above composition, although representative, is only one alternative among many possible metapelitic compositions. It must be kept in mind that other bulk compositions would yield different mineral assemblages and configurations of P-T stability fields.

Partial melting is not depicted on the pseudosections, although it is accounted for in the simulations (see Part II). In the model metapelite system, the beginning of partial melting in the presence of H_2O involves muscovite breakdown and occurs at ~ 700 °C at 0.5 GPa and ~ 750 °C at 1.2 GPa (Vielzeuf and Holloway, 1988). The simplified pseudosection is justified in part by the fact that the spatial extent of partial melting for mid-crustal magmatism is limited, and that melt fractions are < 0.15 . Larger melt fractions reaching ~ 0.3 are predicted for some deep-crustal mafic intrusion scenarios. For these cases, however, peak-T conditions are generally > 800 °C, beyond the T limit of the pseudosection. Nonetheless, the high-T mineral assemblages at $P \geq 0.5$ GPa illustrated on the pseudosection are metastable with respect to melt

Fig. 3. (A) Model P-T-t paths for an overthrust setting with erosion rate 1 mm yr^{-1} (thick lines) and 0.5 mm yr^{-1} (thin lines). In this and all of the subsequent figures the P-T-t paths are for the rock column located at $x = 10 \text{ km}$; points on the paths mark 5 Myr intervals. Initial rock depth (km) shown for each P-T-t path. Dashed line represents beginning of water-saturated partial melting due to muscovite breakdown (Vielzeuf and Holloway, 1988). (B) Representative pseudosection for metapelitic rocks. For simplicity, partial melting relations are not distinguished graphically, but high-T conditions (≥ 725 °C) are highlighted with a stipple pattern on this and most subsequent figures. B: biotite; Ch: chlorite; Crd: cordierite; Ctd: chloritoid; G: garnet; Kfs: K-feldspar; Ky: kyanite; Opx: orthopyroxene; Sil: sillimanite; St: staurolite. (C) Peak-T (T_p) metamorphic assemblages at 35 Myr for a model of regional metamorphism with erosion rate 1 mm yr^{-1} after 35 km of exhumation. P_p denotes pressure at peak temperature (GPa). P_p contours shown with dashed lines (GPa). (D) Peak-T metamorphic assemblages at 70 Myr for a model of regional metamorphism with erosion rate 0.5 mm yr^{-1} after 35 km of exhumation. P_p contours shown with dashed lines (GPa). Note that neither model predicts peak mineral assemblages in the sillimanite zone.

under water-saturated conditions. Consequently, on most diagrams we overlay a stipple pattern on graphical depictions of mineral assemblages at $T \geq 725$ °C to show in a general way where melt would likely have formed in water-bearing systems.

Our treatments of fluid flow, prograde and retrograde metamorphic reactions, and hydrofracturing related to fluid production are briefly summarized here and discussed in greater depth in the Appendix and Part II. We assume that the wall rocks in the crustal section have an interconnected porosity and depth-dependent permeability; the permeability is based on the empirical relationship suggested by Manning and Ingebritsen (1999). The permeability is constant at the surface (10^{-16} m²) and decreases with depth exponentially with the characteristic length scale of 2.5 km to the reference background value of 10^{-19} m² (Lyubetskaya and Ague, 2009a). At higher temperatures, we specify that permeability decreases with increasing temperature using an exponential function that passes through 10^{-19} m² at 700 °C and $\sim 10^{-21}$ m² at 900 °C. This decrease in permeability roughly coincides with the initiation of partial melting in metapelitic rocks. The rocks in the vicinity of and beneath the crust-mantle boundary, as well as magmas and the high-temperature, partial melt-bearing rocks within and around the newly emplaced intrusions, are therefore much less permeable to fluid than fully-crystallized rock.

Perhaps the most important simplification of the fluid flow model is that the porous rock matrix is rigid (it can maintain an open pore network) and thus does not compact with time. This simplification has implications for the fluid flow patterns, as discussed in Part II. However, it is critical to emphasize that the thermal effects of fluid advection are small in the parameter space explored in our models and generally do not exceed 10 °C at the regional scale (Part II). This result will hold true whether compaction is considered or not, as fluid-driven heat transfer depends primarily on the devolatilization fluid flux, the regional length scale of flow, and the thermal conductivity of the rock mass (compare Brady, 1988). The thermal evolution in the models presented below is therefore dominated by the heat advection of magma emplacement, and thermal conduction away from the magmas into the surrounding rocks.

RESULTS

Model P-T-t Paths and Peak Metamorphic Mineral Assemblages

Regional metamorphic P-T-t paths for an overthrust setting with the average values of radiogenic and basal heating in the absence of magmatism are illustrated in figure 3A. In this and all subsequent figures, the P-T-t paths are for a rock column located at $x = 10$ km. The “peak” conditions are assessed as the maximum or peak temperature (T_p) developed by a model rock unit during its exhumation history and the pressure (P_p) at which this peak temperature was attained.

The lack of additional heat sources in this model in conjunction with the relatively fast erosion rate of 1 mm yr⁻¹ results in peak metamorphic temperatures below 700 °C for the bulk of the crustal section. The timescale over which the rocks are at or near peak thermal conditions is characteristically large: rock temperatures are maintained within 10 °C of their peak values for at least 5 to 7 Myr. At a slower erosion rate of 0.5 mm yr⁻¹ the model P-T-t paths reach higher temperatures, as the longer exhumation history (70 Myr instead of 35 Myr) allows more time for production of heat by crustal radioactive sources. The peak temperature timescale is correspondingly increased to more than 10 Myr. Peak temperature attainment is not synchronous for rocks located at different depths: shallow rocks will reach their peak temperatures sooner than deep rocks by about 5 Myr for every 10 km of depth increment. There is also a noticeable increase in the pressures at which peak temperatures are attained for deeper rocks as opposed to shallower ones: the total pressure difference within the lower plate of the thrust at the end of the simulation reaches 0.3 GPa.

Figures 3C and 3D present reconstructions of peak T mineral assemblages at the end of simulation for erosion rates of 1 mm yr^{-1} and 0.5 mm yr^{-1} . In this and all subsequent reconstructions, the mineral assemblages depicted: 1) are based on the pseudosection in figure 3B and 2) are the maximum T assemblages that have formed up to and including the time of the model time slice. A given assemblage is no longer updated during cooling after the rock has reached its peak T. Consequently, retrograde mineral assemblages are not illustrated. On most diagrams, we also show the $725 \text{ }^\circ\text{C}$ contour and graphically overlay a stipple pattern on rocks that reached $T > 725 \text{ }^\circ\text{C}$ to illustrate in a general way where partial melting of metapelitic wallrock would be expected. Importantly, the rocks in these high-T regions did not reach peak-T conditions simultaneously; the diagrams show all rocks that reached these conditions at times up to and including the model time slice. Regions characterized by T or peak T attainment at $<500 \text{ }^\circ\text{C}$, $<0.25 \text{ GPa}$, or $>800 \text{ }^\circ\text{C}$ are not shown in detail.

Thermal relaxation of the overthickened crust leads to the formation of a vertical sequence of peak mineral assemblages from the low-grade index minerals of the chlorite and biotite zones in the shallower parts of the crust, through the staurolite and kyanite zones, to the high-pressure, high-temperature garnet-biotite zone (without chlorite) at the base of the crust. Although not directly depicted on the pseudosection, some partial melt and an aluminosilicate phase would be expected in this zone at $T \geq 750 \text{ }^\circ\text{C}$ and $P \geq 1 \text{ GPa}$ due to reactions involving muscovite breakdown in the presence of H_2O (Vielzeuf and Holloway, 1988). At the slower erosion rate of 0.5 mm yr^{-1} , the peak temperatures within the thrust core are noticeably higher than in the case with faster erosion; at 35 Myr temperatures of rocks below 30 km exceed $800 \text{ }^\circ\text{C}$. Importantly, however, no intermediate pressure ($\sim 0.4\text{--}0.6 \text{ GPa}$), amphibolite facies sillimanite zone mineral assemblages are produced in these amagmatic models, in contrast to the common occurrence of the sillimanite zone in field settings worldwide.

For both erosion rates, the peak mineral assemblage fields on the flank of the thrust (between 60 and 120 km in the x direction) plunge downward reflecting the decrease in metamorphic temperatures as a response to the reduced crustal thickness in this area. The resulting compression of the mineral assemblage fields leads to the significant, non-isobaric Metamorphic Field Temperature Gradient (MFTG) in this area; the transition from high-grade rocks in the core of the thrust to the low-grade rocks at the flanks takes place over a lateral distance of about 20 to 40 km. This distance may be even smaller for steeper fault zones between the two colliding plates.

The effects of deep mafic magmatism on regional P-T-t paths and peak mineral assemblages for an overthrust model with erosion rate 1 mm yr^{-1} are illustrated in figures 4, 5 and 6. Magmatic intrusion consists of 10 sills 500 m thick emplaced randomly in the depth range of 35 to 50 km every 20,000 years ("fast intrusion"; emplacement rate of 2.5 cm yr^{-1}) or 200,000 years ("slow intrusion"; emplacement rate of 0.25 cm yr^{-1}) at $1200 \text{ }^\circ\text{C}$. For the faster emplacement rate, the intrusion of 5 km of mafic magma takes 0.2 Myr, whereas slow intrusion occurs over 2 Myr. For the model presented in figure 4, magmatism begins immediately after the start of exhumation at 0 Myr. Figures 4A and 4B demonstrate the very strong influence of the early magmatism on the metamorphic P-T-t paths. Even those rocks that were above or below the depth range of intrusion attain peak temperatures at least $50 \text{ }^\circ\text{C}$ higher than in the absence of magmatism. The intrusion of magma leads to the downward displacement of rocks located below the magmatism region initially at depths of $>50 \text{ km}$; the maximum displacement is in the center of the thrust zone and equals 5 km. The enhanced depth and the corresponding increase in pressure during the first 1 to 2 Myr are reflected in the form of the P-T-t paths. At the end of the simulation, the deepest rocks are located 5 km below their corresponding positions in a model without magmatism (dashed lines in fig. 4A, B). The peak temperature timescales are consider-

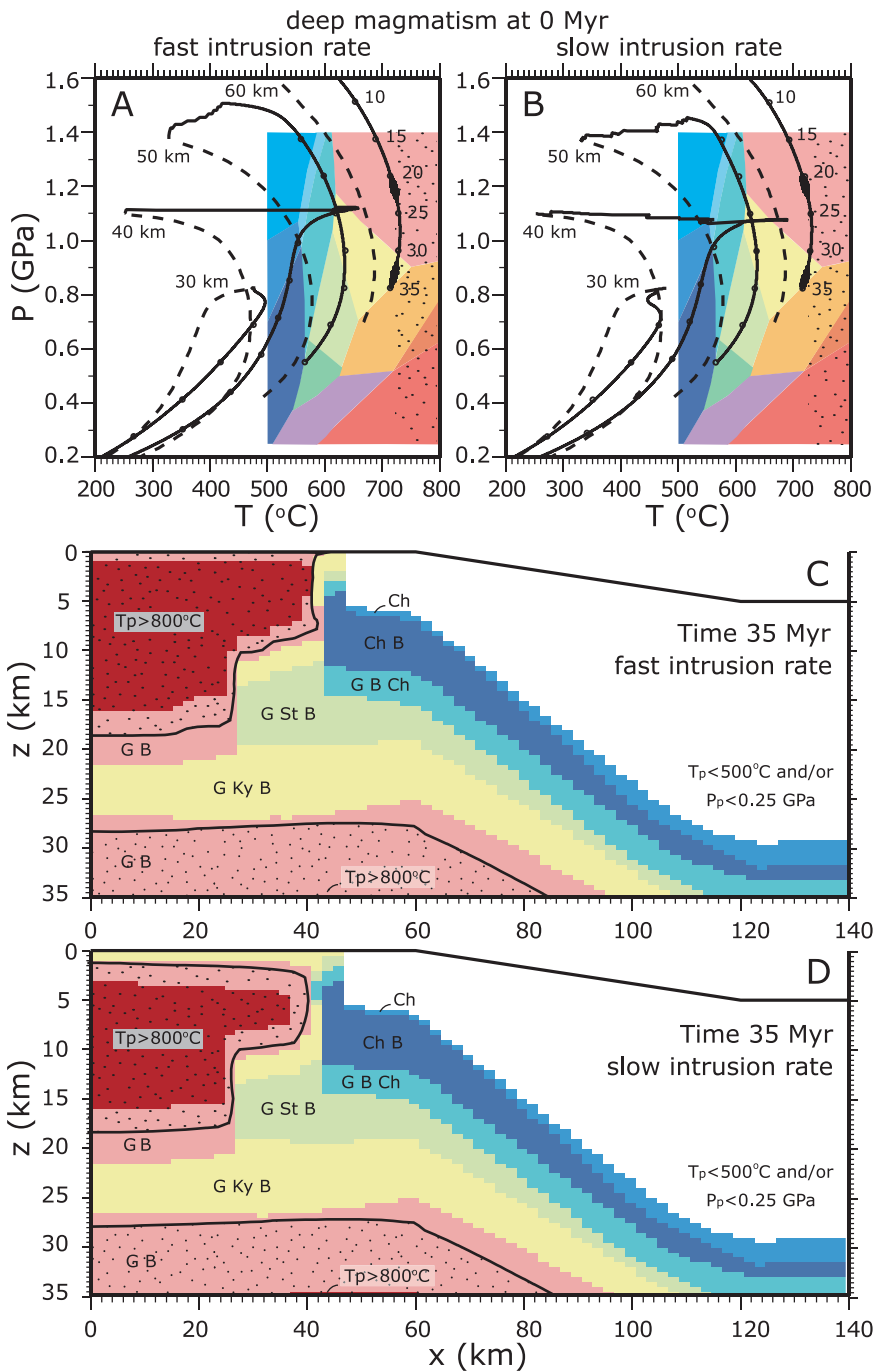


Fig. 4. (A) Model P-T-t paths for erosion rate 1 mm yr^{-1} in the absence of magmatism (dashed lines) and for a model with 10 mafic sills 500 m thick intruded every 20 kyr in the depth interval of 35–50 km initiated at 0 Myr (solid lines). In this and subsequent figures small temperature fluctuations at $\sim 715^\circ\text{C}$ are related to the initiation or termination of partial melting in metapelitic rocks and result from the relatively sparse numerical grid and the shape of the melting function (Appendix). (B) Same as A, but magmatic sills are intruded every 200 kyr. (C) Peak metamorphic assemblages at 35 Myr for model in part A. Rocks that reached $T \geq 725^\circ\text{C}$ are shown with a stipple pattern bordered by the 725°C contour. These conditions were reached some time prior to or including the model time. Thus the contours and stipple pattern do not represent the T field at 35 Myr. (D) Peak metamorphic assemblages at 35 Myr for model in part B.

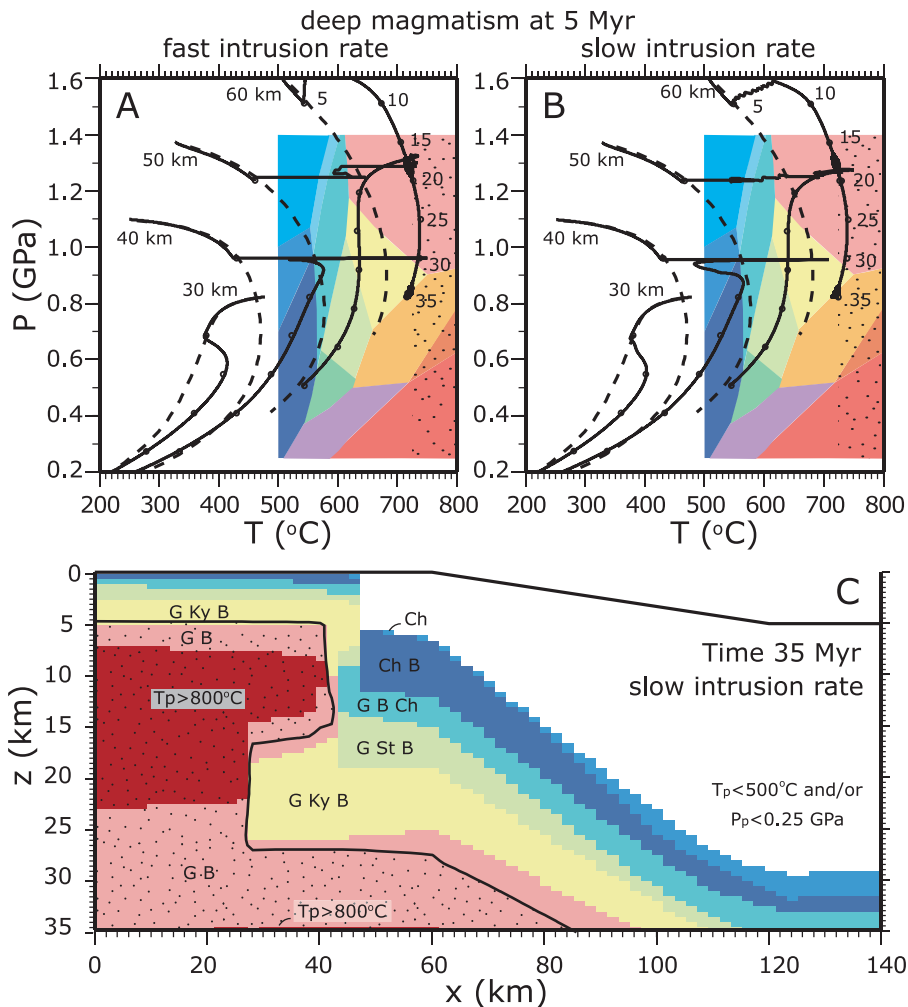


Fig. 5. (A) Model P-T-t paths for erosion rate 1 mm yr⁻¹ in the absence of magmatism (dashed lines) and for a model with 10 mafic sills 500 m thick intruded every 20 kyr in the depth interval of 35–50 km beginning at 5 Myr (solid lines). (B) Same as A, but sills are intruded every 200 kyr. (C) Peak metamorphic assemblages at 35 Myr for model in part B. Note 725 °C contour and rocks that reached T ≥ 725 °C (stipple pattern).

ably reduced in comparison to the model with no magmatism: rocks in the vicinity of intrusions are within 10 °C of their peak temperatures for only a few hundred thousand years. The peak temperature buildup time is about 2 Myr in a model with slow intrusion compared to that in the fast intrusion case, about 0.2 Myr.

The difference in the rates of emplacement affects the form of the P-T-t paths, but does not significantly alter the peak metamorphic assemblages. In both cases the core of the thrust at 35 Myr is composed of rocks that reached 725 °C or more (fig. 4C, D). At earlier times these high-grade rocks had been capped by rocks with lower-T mineral assemblages, from chlorite-biotite through staurolite to kyanite zone, as in the metamorphic sequence characteristic for regional metamorphism in the absence of magmatism (fig. 3C). By 35 Myr, these rocks have been removed from the model crustal section by

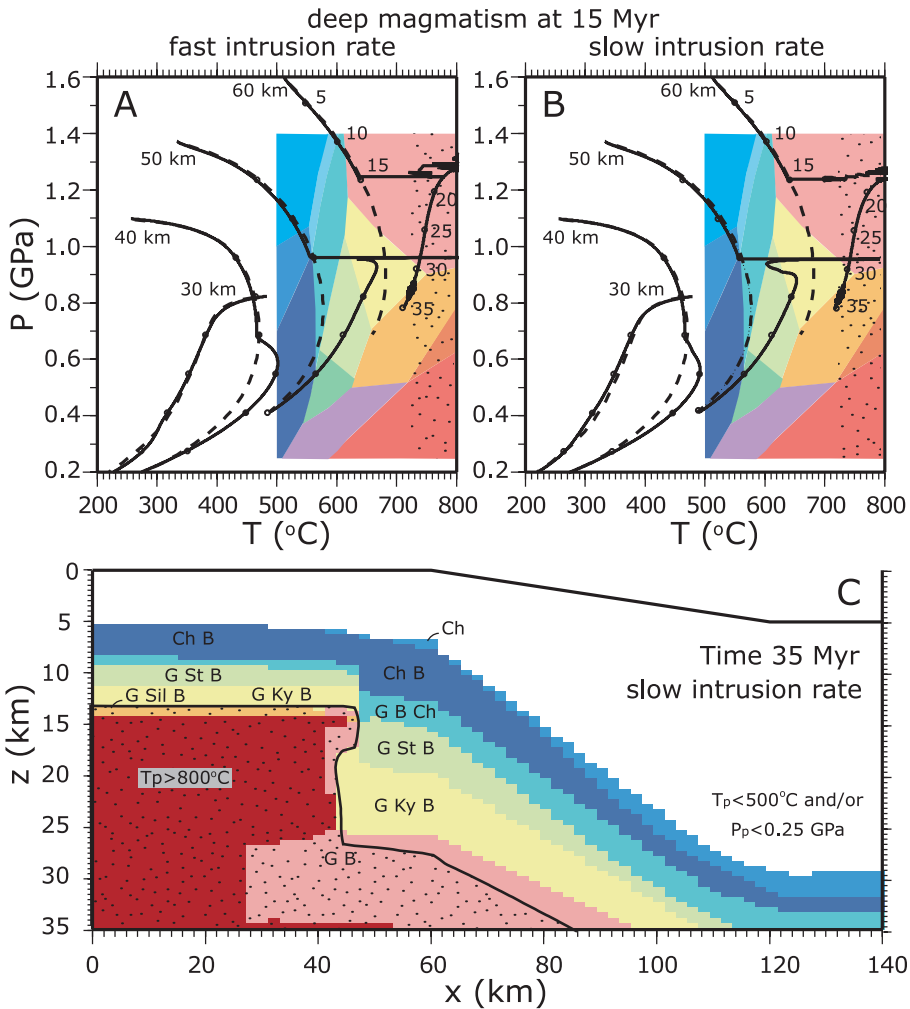


Fig. 6. (A) Model P-T-t paths for erosion rate 1 mm yr^{-1} in the absence of magmatism (dashed lines) and for a model with 10 mafic sills 500 m thick intruded every 20 kyr in the depth interval of 35–50 km beginning at 15 Myr (solid lines). (B) Same as A, but sills are intruded every 200 kyr. (C) Peak metamorphic assemblages at 35 Myr for model in part B. Note 725°C contour and rocks that reached $T \geq 725^\circ\text{C}$ (stipple pattern).

surface erosion. Relatively minor differences in the spatial distribution of peak metamorphic mineral assemblages for the intrusion rates of 0.25 cm yr^{-1} and 2.5 cm yr^{-1} are characteristic for other models with similar magmatism parameters (10 sills with thickness of 500 m); we will only show the 2-D diagrams for the slower intrusion rate in the subsequent figures.

Figures 5 and 6 illustrate the model results for deep magmatism that begins at 5 Myr and 15 Myr after the start of exhumation, respectively. By 5 Myr, the initially inverted geotherm in the core of the thrust is eliminated and up to 5 km of the crustal rock are removed by erosion in the faulted section of the model. Rocks that were initially at 40 to 55 km depth are, at 5 Myr, brought into the 35 to 50 km depth interval of magmatic intrusion. The temperature of the wall rock during sill emplacement is

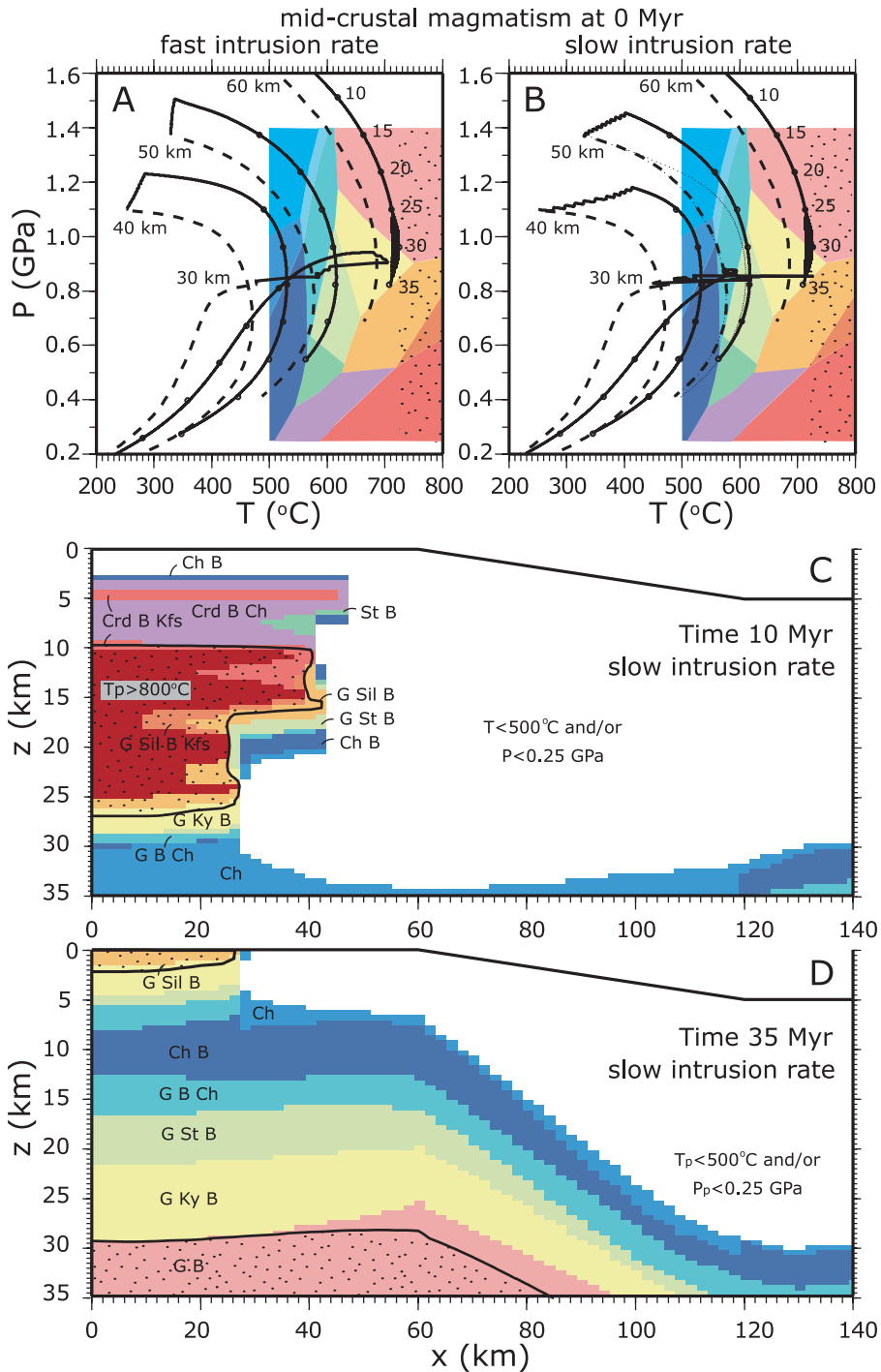


Fig. 7. (A) Model P-T-t paths for erosion rate 1 mm yr^{-1} in the absence of magmatism (dashed lines) and for a model with 10 mafic sills 500 m thick intruded every 20 kyr in the depth interval of $15\text{--}35 \text{ km}$ beginning at 0 Myr (solid lines). (B) Same as A, but sills are intruded every 200 kyr . (C) Mineral assemblages at 10 Myr for model in part B. Note $725 \text{ }^\circ\text{C}$ contour and rocks that reached $T \geq 725 \text{ }^\circ\text{C}$ (stipple pattern). (D) Peak metamorphic assemblages at 35 Myr for model in part B.

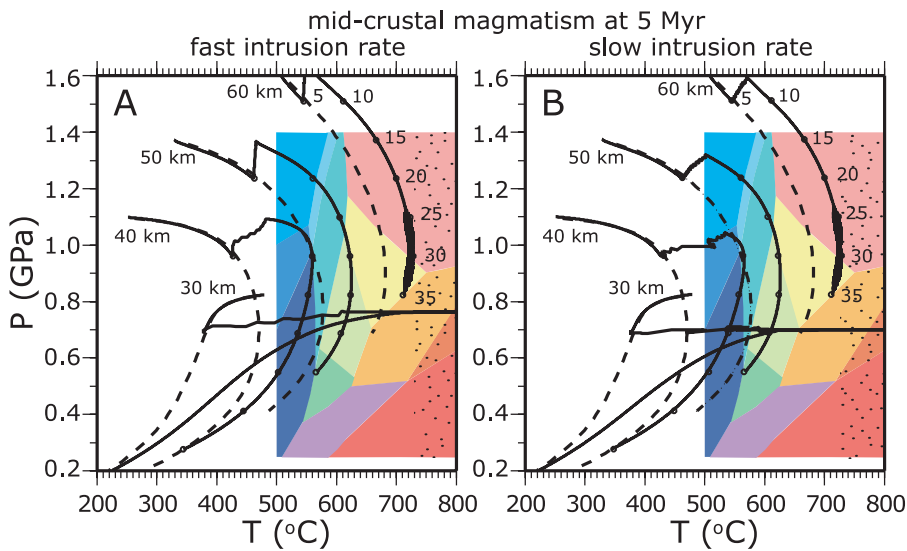


Fig. 8. (A) Model P-T-t paths for erosion rate 1 mm yr^{-1} in the absence of magmatism (dashed lines) and for a model with 10 mafic sills 500 m thick intruded every 20 kyr in the depth interval of 15–35 km beginning at 5 Myr (solid lines). (B) Same as A, but sills are intruded every 200 kyr.

therefore considerably higher than in the previous model with magmatism at 0 Myr (compare fig. 4A, B and fig. 5A, B). This translates into a larger volume of rocks that attained temperatures in excess of $800 \text{ }^\circ\text{C}$ by the end of the simulation (compare figs. 4D and 5C). Furthermore, the lower-grade chlorite and biotite zone rocks that cap the high-P, high-T garnet-biotite assemblages in the core of the thrust are preserved within the crustal section at 35 Myr.

For magmatism commencing at 15 Myr, crustal rocks in the model overthrust section are almost half-way through their ascent to the surface; the base of the crust at this time is at 55 km. Magmatic intrusion in the depth interval of 35 to 50 km now has the strongest effect on the rocks that were initially as deep as 50 to 65 km (fig. 6A, B). The sequence of peak metamorphic mineral assemblages in this model generally repeats those in other models with deep magmatism (compare fig. 6C with figs. 4D and 5C). In this case, however, because of the relatively late initiation of intrusion the magmatic source of heat is located at the very bottom of the crust. High-grade rocks are brought to the model surface if deep magmatism starts early in the exhumation history (fig. 4C, D). On the other hand, lower-grade rocks are exhumed when magmatism begins later (figs. 5C, 6C).

The intrusion of 10 individual mafic sills of 500 m thickness at mid-crustal depths of 15 to 35 km is documented in figures 7, 8, and 9. Figure 7 presents the P-T-t paths and the mineral assemblage distributions for a model with mid-crustal magmatism that started simultaneously with the beginning of exhumation at 0 Myr. The early thermal event leads to dramatic increases in rock peak temperatures at shallow and mid-crustal depths. The thermal effect of magmatism on deeper rocks (initially at 50 or 60 km) is also clear. In this case, however, the increase in peak temperatures is mainly the result of displacement of P-T-t paths towards greater depths rather than a direct consequence of heating from intruded magma. In figure 7C we show the spatial distribution of metamorphic mineral assemblages at 10 Myr after the beginning of the simulation, corresponding to ~ 8 Myr after the end of magmatism with slow emplacement rate. Considerable volumes of rock affected by magmatic intrusion develop mineral assem-

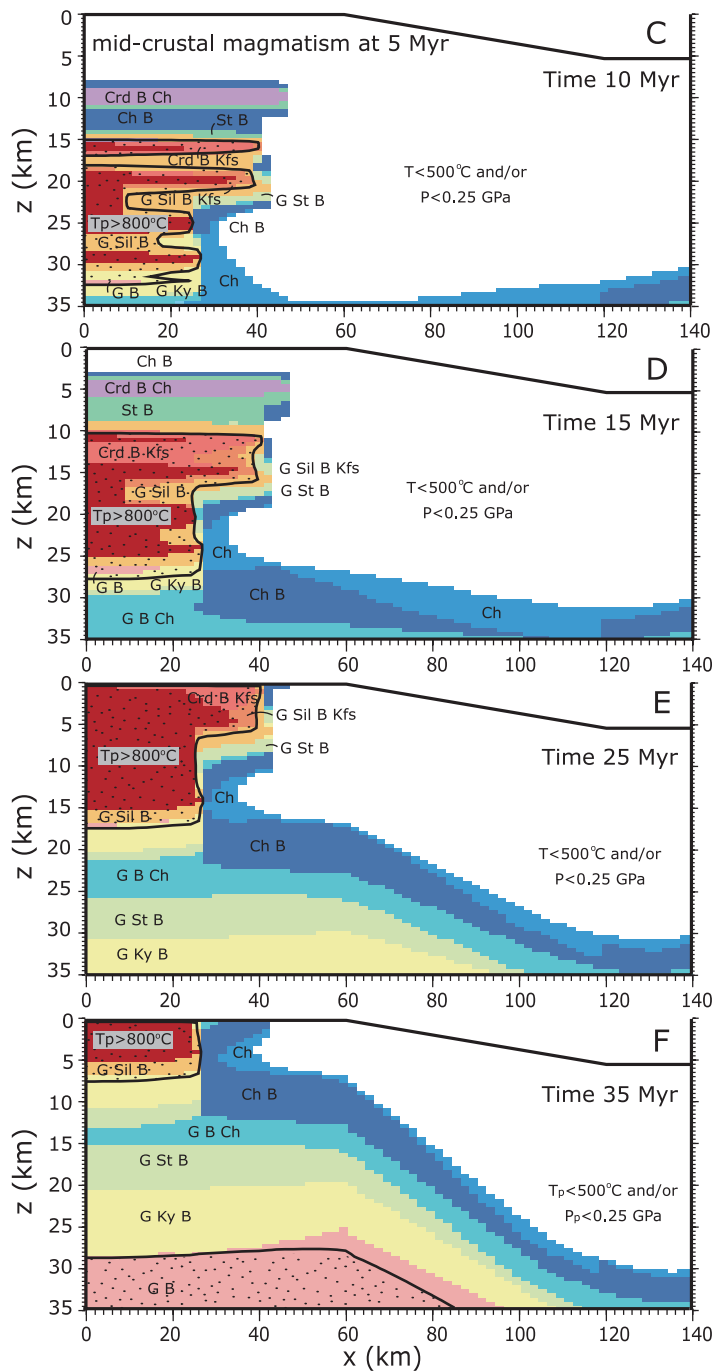


Fig. 8. Continued (C) Mineral assemblages at 10 Myr for model in part B. Note 725 °C contour and rocks that reached $T \geq 725$ °C (stipple pattern). (D) Mineral assemblages at 15 Myr for model in part B. E. Mineral assemblages at 25 Myr for model in part B. F. Peak metamorphic assemblages at 35 Myr for model in part B.

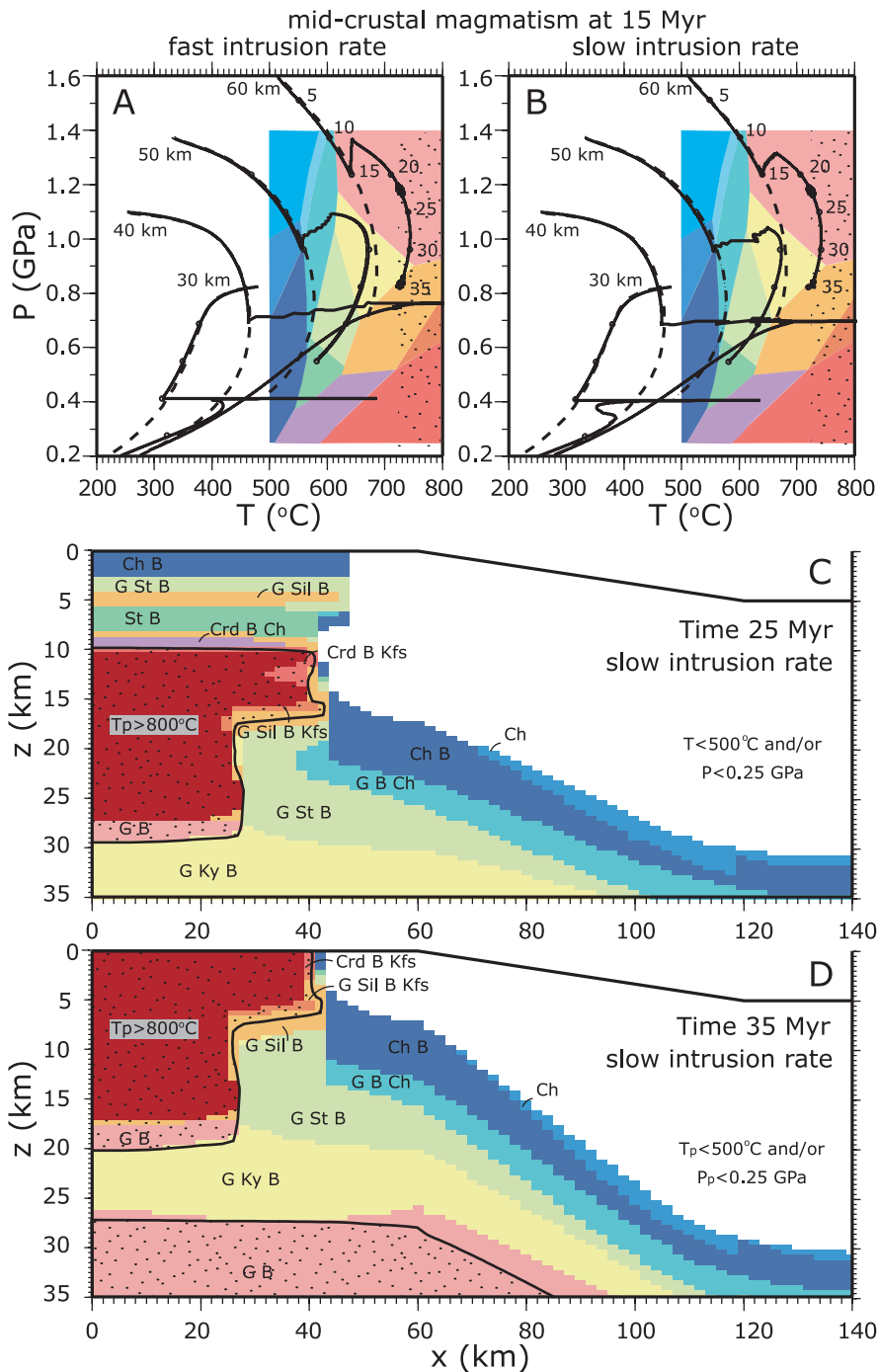


Fig. 9. (A) Model P-T paths for erosion rate 1 mm yr^{-1} in the absence of magmatism (dashed lines) and for a model with 10 mafic sills 500 m thick intruded every 20 kyr in the depth interval of $15\text{--}35 \text{ km}$ beginning at 15 Myr (solid lines). (B) Same as A, but sills are intruded every 200 kyr . (C) Metamorphic mineral assemblages at 25 Myr for model in part B. Note $725 \text{ }^\circ\text{C}$ contour and rocks that reached $T \geq 725 \text{ }^\circ\text{C}$ (stipple pattern). (D) Peak metamorphic assemblages at 35 Myr for model in part B.

blages characteristic of LP/HT metamorphism at 5 to 10 km depth, including cordierite-biotite-K-feldspar. Magmatic intrusion into the shallow, low-temperature crustal rock leads to fast cooling of emplaced magmas and to their crystallization in less than 5,000 years (that is, single time-step in our models). Consequently, only rocks in the lower part of the magmatism region (>10 km depth at 10 Myr) record regional temperatures in excess of 800 °C.

After 35 Myr of exhumation all the upper plate rocks of the thrust section with LP/HT metamorphic signatures are removed by erosion (fig. 7D). Below about 10 km depth, the remaining crustal section is composed of rocks with peak mineral assemblages very similar to those produced by regional metamorphism in the absence of magmatism (fig. 3C, D). Note, however, that sillimanite zone rocks are at the surface for the magmatic case (fig. 7D), whereas for the comparable amagmatic model the top of the metamorphic sequence is still buried at 7 to 8 km depth and is in the chlorite or biotite zone (fig. 3C).

The thermal effects of mid-crustal magmatism that begins at 5 Myr after that start of the simulation are illustrated in figure 8. As in the case of deep magmatism, when intrusion is initiated at later times in the model evolution, the emplacement of magma occurs into the ambient rock at higher temperatures than in the models of early intrusion. This affects the form of the P-T-t paths and the width of the thermal peaks, as well as the spatial distribution of peak metamorphic mineral assemblages. In figures 8C–F we show the temporal evolution of mineral assemblages within the upper 35 km of the model thrust section. The disjoint bands of rock with high-T mineral assemblages that mark the areas of sill emplacement after the end of magmatism (cordierite-biotite-K-feldspar, garnet-sillimanite-biotite-K-feldspar and assemblages with peak T above 800 °C) expand with time and join into larger fields due to thermal conduction. At the same time, the entire section of thickened crust continuously moves upward with exhumation. As shown in figure 8F, below the depth interval of magmatism in the lower part of the thickened crustal section, a higher-P sequence of index minerals characteristic for regional metamorphism, that is, staurolite, kyanite, and garnet-biotite (without chlorite), develops as a result of thermal relaxation of the overthickened crust.

Finally, figure 9 shows the results for models with mid-crustal magmatism initiated at 15 Myr after the beginning of simulation. The increased temperature of the wall rock at the start of the intrusion leads to the development of a large zone of rocks metamorphosed at temperatures in excess of 800 °C. This zone is capped by rocks that contain the Buchan-type LP/HT index mineral cordierite (fig. 9C). By the end of the simulation, however, these rocks are removed from the model crust section by surface erosion.

The above models predict the effects of magmatic intrusion at an erosion rate of 1 mm yr⁻¹. The impact of different erosion rates is illustrated in figure 10. A magmatic event involving the intrusion of 10 individual sills 500 m thick emplaced every 200,000 years begins at 10 Myr in a model with erosion rate = 0.5 mm yr⁻¹, and at 3.33 Myr in a model with erosion rate = 1.5 mm yr⁻¹; the magmatism duration in both cases is 2 Myr. An identical configuration of random numbers for the depth and the lateral dimension of each sill was used in both cases. The difference in the time gap between the beginning of exhumation and the start of magmatism in the two models reflects the three-fold difference in the timescale of exhumation: 70 Myr for the erosion rate of 0.5 mm yr⁻¹ and ~24 Myr for the erosion rate of 1.5 mm yr⁻¹. By the time magmatism begins, the maximum crustal thickness in the thrust zone in both cases is 65 km; the depth range of magmatism (15–35 km) comprises rocks that were initially at 20 to 40 km.

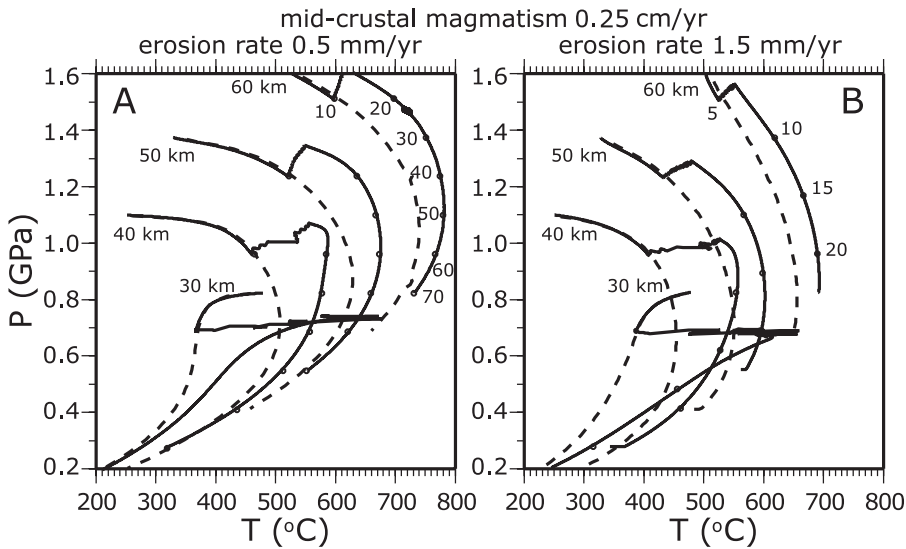


Fig. 10. (A) Model P-T-t paths for erosion rate 0.5 mm yr^{-1} in the absence of magmatism (dashed lines) and for a model with 10 mafic sills 500 m thick intruded every 200 kyr in the depth interval of 15–35 km beginning at 10 Myr (solid lines). (B) Model P-T-t paths for erosion rate 1.5 mm yr^{-1} in the absence of magmatism (dashed lines) and for a model with 10 basaltic sills 500 m thick intruded every 200 kyr in the depth interval of 15–35 km beginning at 3.3 Myr (solid lines).

Although the rates, the depth, and the duration of magmatism are identical in the two models, the P-T-t paths show considerable differences (fig. 10A, B). These differences reflect the very dissimilar ratio of the magmatism duration to the total exhumation history in each model. At the fast erosion rate, the period of magmatism lasts for about 1/12 of the exhumation history of a model rock. Thus, after the thermal peak is attained, temperature drops off over a fairly broad depth/pressure range in the P-T-t paths for rocks in the vicinity of intrusions (fig. 10B). For the slow erosion rate, the duration of magmatism encompasses only 1/34 of the rock exhumation history and, thus, the thermal anomaly spans a narrower depth/pressure range (fig. 10A). Furthermore, at faster erosion rates, the rapid ascent and cooling of exhumed rock counteracts the thermal effect produced by the downward displacement of rocks underneath the magmatism area. The elevation of peak metamorphic temperatures by magmatism within the deep rocks is therefore less in the model with fast erosion than in the model with slow erosion.

The vertical sequence of peak metamorphic mineral assemblages in the two models roughly repeats the one presented on figures 8C–F for erosion rate 1 mm yr^{-1} (not shown). Large volumes of rock in the core of the thrust affected by magmatism develop peak mineral assemblages in the garnet-sillimanite-biotite zone, with smaller amounts of LP/HT mineral assemblages that include cordierite. In the relatively colder model with fast erosion, however, the LP/HT assemblages and rocks with $T_p > 800 \text{ }^{\circ}\text{C}$ are reduced in volume in comparison to models with erosion rates of 1 mm yr^{-1} or 0.5 mm yr^{-1} .

The Effect of Magma Emplacement Mechanism

Our default models of magmatism assume that magma emplacement is accommodated by the vertical downward displacement of the rock column underlying intrusion (fig. 2C, D). This mechanism leads to the progressive transfer of rock beneath the

magmatism zone toward deeper levels, and to the corresponding crustal thickening. In figure 11 we illustrate the model results for the alternative intrusion mechanism: the magma is simply emplaced into the existing wall rock, without its displacement (fig. 2A, B).

The emplacement mechanism can have a significant impact on P-T-t paths. For a model of mid-crustal magmatism initiated at 15 Myr consisting of 10 mafic sills intruded every 200,000 yr, the elevation of peak metamorphic temperatures by magmatism is much less in a model without wall rock displacement (fig. 11A, C) than for a model with displacement (fig. 9B, C). In the default models, the wall rock displacement towards deeper levels of the crust transfers crustal isotherms downward. This process works against the exhumation, which brings model isotherms closer towards the surface and thus facilitates rock cooling. Intruded magma therefore tends to cool down more slowly in the model with wall rock displacement compared to the model without displacement. As a result, the metamorphic peak temperatures of rocks in the vicinity of intrusions in figure 11A are much lower than in the default model, figure 9B. The lower peak temperatures in the model without displacement are also reflected in the mineral assemblage map on figure 11C: only wall rocks in the vicinity of the deepest sills record temperatures in excess of 800 °C. The noticeable inflections toward higher pressures that are produced in the deep rock P-T-t paths on figure 9B by rock burial during intrusion are absent from the P-T-t paths on figure 11A. On the contrary, exhumation leads to the progressive decrease in rock depth during the period of magmatism. Consequently, the peak temperatures of deep rocks are also considerably diminished in comparison to the default model.

In figures 11B and 11D we show the results for a model without wall rock displacement and with a two-fold increase in the number of sill intrusions: 20 instead of 10. The peak temperatures and the peak mineral assemblages in this model are close to those in our default model with 10 sills 0.5 km thick (fig. 9B, C). The volume-for-volume emplacement mechanism, therefore, may lead to removal by accelerated cooling of almost half of the thermal energy provided by magmatism. It must be noted, however, that magmatism in the shallow parts of the crust is likely to be accompanied by upwards movement of rock lying on top of the intruded magma (compare Jónsson and others, 2005). Although we do not specifically model this situation, our results imply that such an emplacement scenario will facilitate faster cooling of plutons and the surrounding wall rock and impede the attainment of high peak temperatures in the shallow crust.

Variations in Temperature, Rate of Magma Emplacement, and Sill Thickness

In this section we illustrate some of the relationships between regional metamorphism and syn-metamorphic intrusion parameters, such as the rate and the temperature of magma emplacement and the spatial dimensions of magmatic sills (figs. 12 and 13). In figures 12A and 12B we show the mineral assemblages for our default configuration of magmatic sills (10 sills, each 500 m thick) emplaced at mid-crustal depths at 5 Myr after the start of the simulation. In contrast to the earlier models in which the lateral dimensions of the mafic sills vary between 10 to 50 km from the left boundary (for example, fig. 8), the sills in figures 12A and 12B are narrower, having lateral dimensions of about 6 to 10 km. Predictably, narrow sills intruded into the relatively low-temperature wall rock tend to cool faster than sills with larger lateral dimensions; their thermal effect on the ambient rock is thus also diminished. As a result, the volume of rock that develops mineral assemblages in the granulite facies of metamorphism (peak temperatures exceeding 800 °C) is reduced compared to a similar model with larger sills (fig. 8C, D).

It is important to point out the very strong lateral metamorphic gradients in the vicinity of intrusion in this model as well as in many of the above models. In particular,

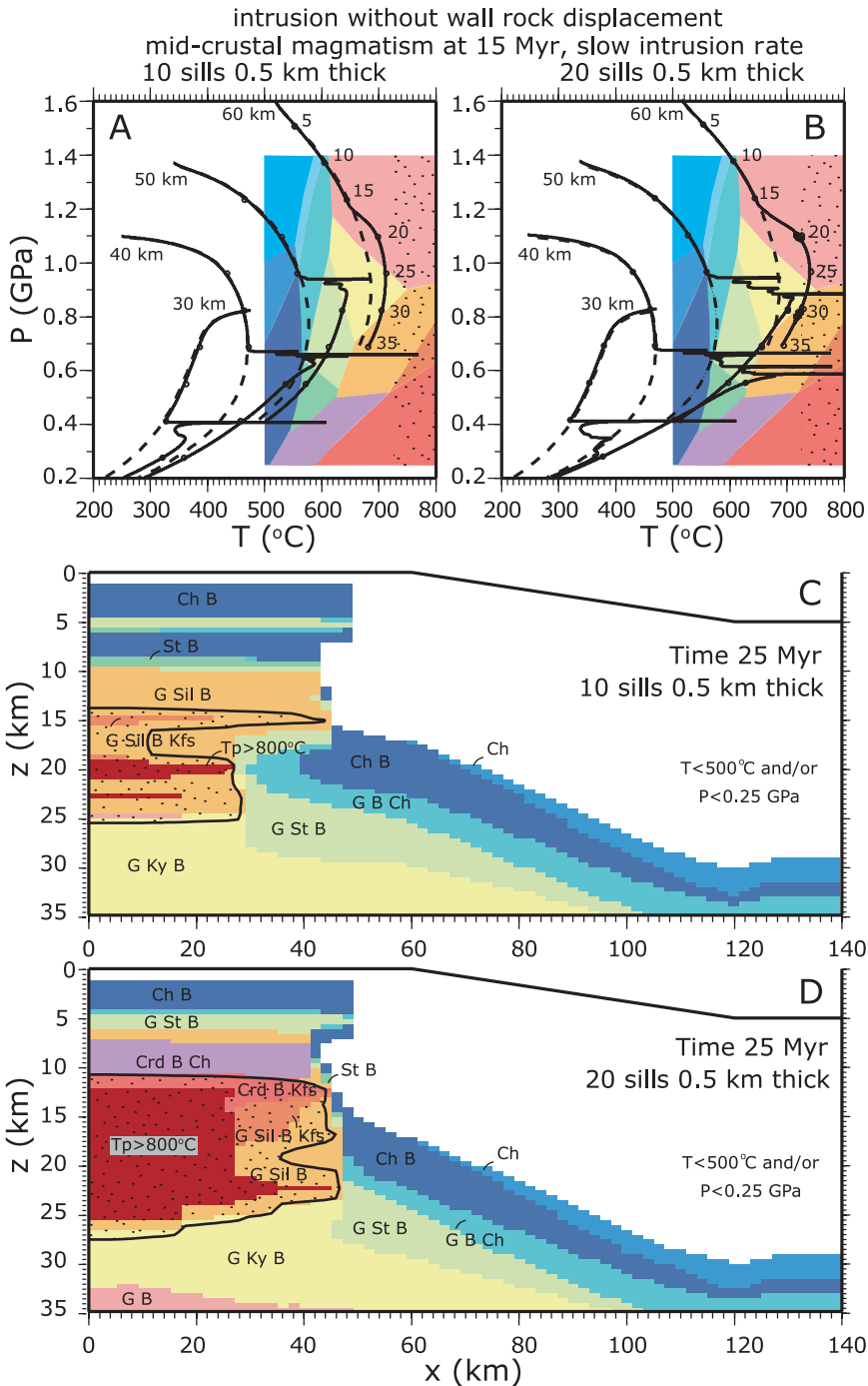


Fig. 11. Model results for the alternative magma emplacement mechanism, in which no wall rock displacement occurs during intrusion. (A) Model P-T-t paths for erosion rate 1 mm yr^{-1} in the absence of magmatism (dashed lines) and for a model with 10 mafic sills 500 m thick intruded every 200 kyr in the depth interval of 15–35 km beginning at 15 Myr (solid lines). (B) Model P-T-t paths for erosion rate 1 mm yr^{-1} in the absence of magmatism (dashed lines) and for a model with 20 mafic sills 500 m thick intruded every 200 kyr in the depth interval of 15–35 km beginning at 15 Myr (solid lines). (C) Mineral assemblages at 25 Myr for model in part A. Note 725°C contour and rocks that reached $T \geq 725^\circ\text{C}$ (stipple pattern). (D) Mineral assemblages at 25 Myr for model in part B.

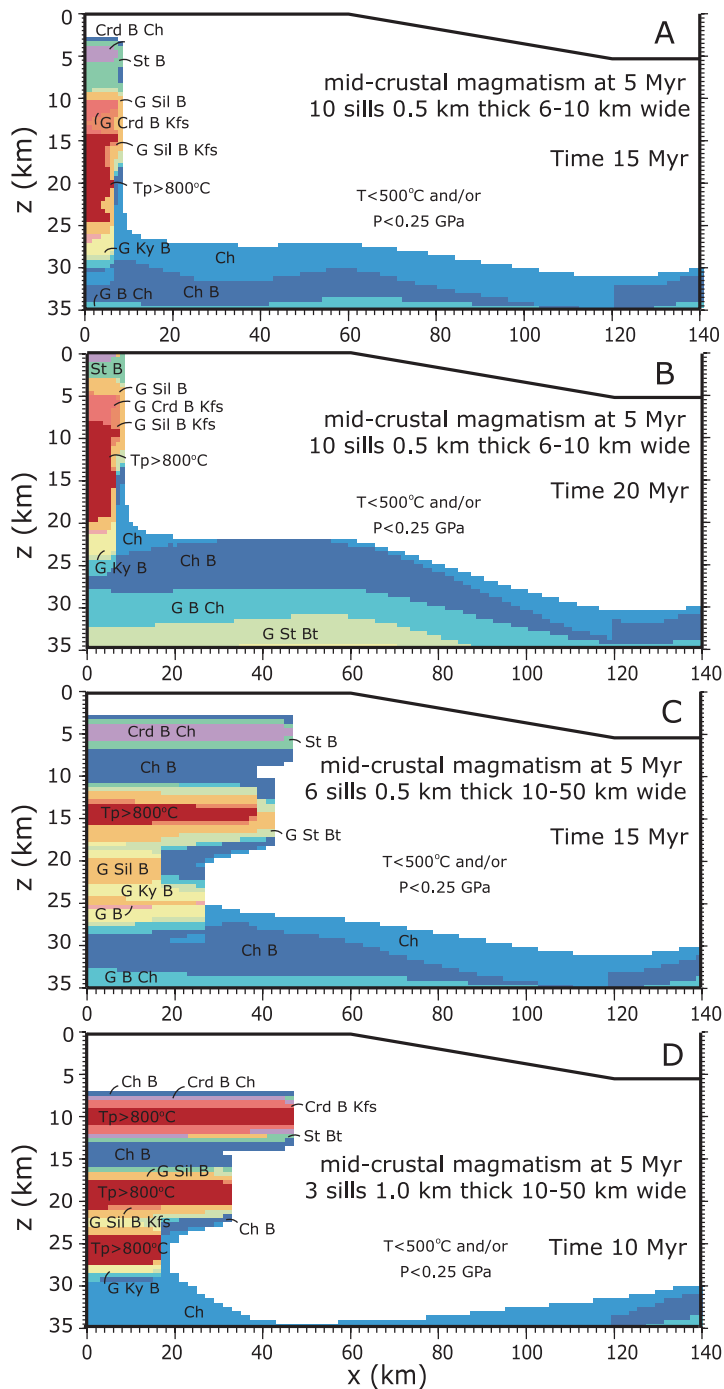


Fig. 12. Model results for a range of sill widths and thicknesses. Stipple pattern for rocks that attained $T \geq 725^\circ\text{C}$ omitted for clarity. (A) Prograde mineral assemblages at 15 Myr for a model with 10 mafic sills 500 m thick intruded every 200 kyr in the depth interval of 15–35 km beginning at 5 Myr; lateral dimensions of sills vary between 6 and 10 km. (B) Metamorphic mineral assemblages at 20 Myr for model in part A. (C) Mineral assemblages at 15 Myr for a model with 6 mafic sills 500 m thick intruded every 200 kyr in the depth interval of 15–35 km beginning at 5 Myr; lateral dimensions of sills vary between 10 and 50 km. (D) Mineral assemblages at 10 Myr for a model with 3 mafic sills 1 km thick intruded every 200 kyr in the depth interval of 15–35 km beginning at 5 Myr; lateral dimensions of sills vary between 10 and 50 km.

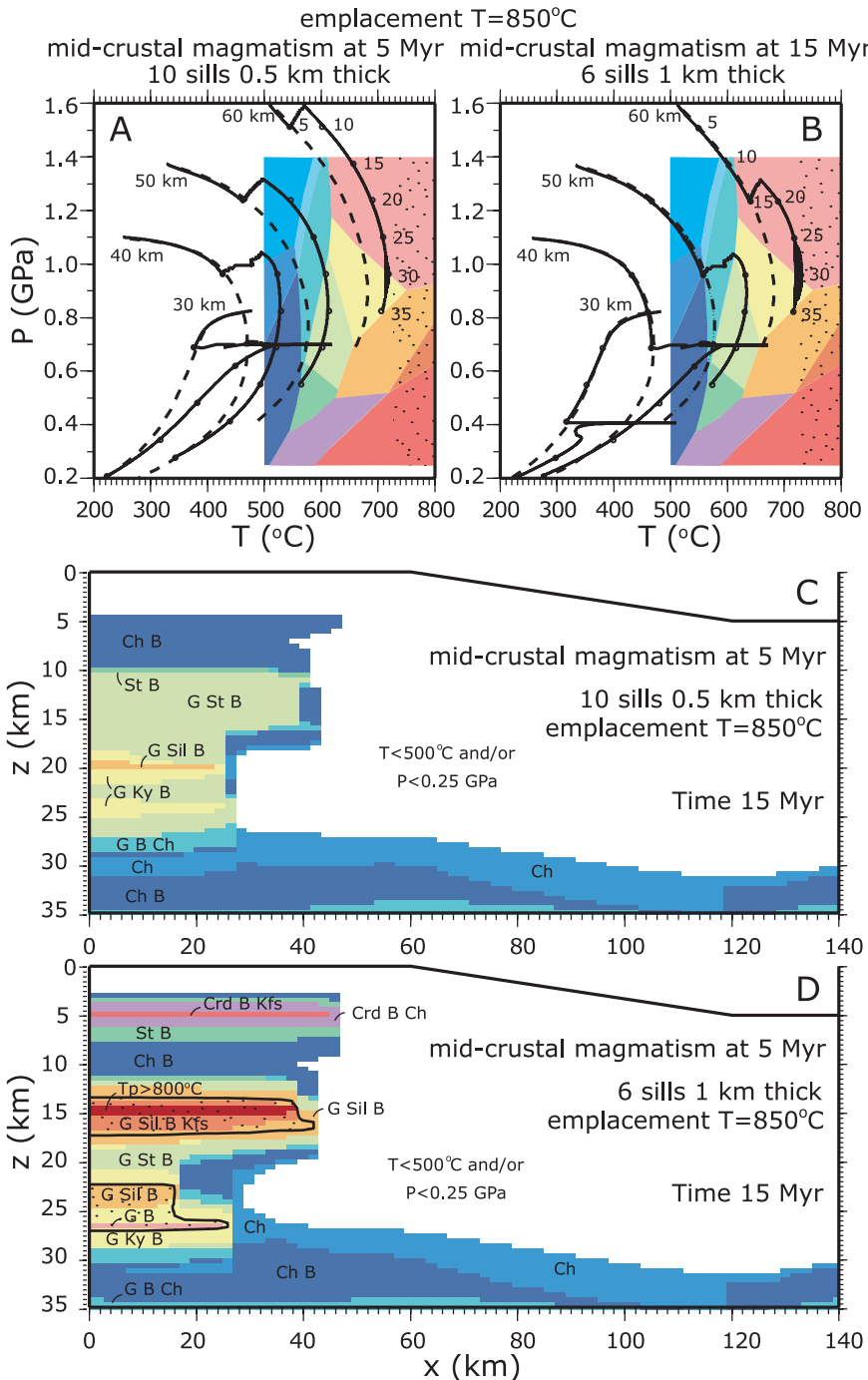


Fig. 13. (A) Model P-T-t paths for erosion rate 1 mm yr^{-1} in the absence of magmatism (dashed lines) and for a model with 10 intermediate-felsic sills 500 m thick (emplacement temperature 850°C) intruded every 200 kyr in the depth interval of 15–35 km beginning at 5 Myr (solid lines). (B) Same as A, but magmatic intrusion consists of 6 intermediate-felsic sills 1 km thick. (C) Metamorphic mineral assemblages at 15 Myr for model in part A. (D) Mineral assemblages at 15 Myr for model in part B. Note 725°C contours and rocks that reached $T \geq 725^{\circ}\text{C}$ (stipple pattern).

note the area adjacent to the center of the magmatism region at ~ 15 km depth at 15 Myr, and at 5 km depth at 20 Myr (fig. 12A, B). The transition from sillimanite zone to the chlorite zone and minerals with $T_p < 500$ °C takes place within the lateral distance of only 1 km. Such steep gradients in peak metamorphic temperatures in the flanks of intrusion are the result of the large contrasts between the emplaced magma temperature (1200 °C) and the temperature of the wall rock (< 400 °C). Intrusion into the cold environment leads to very fast cooling of magmatic sills and relatively little heat conduction into the surrounding rock. As a result, the wall-rock temperature is only moderately elevated at short distances from the intrusion, whereas rocks in close proximity to the magmatic sills, though rapidly cooling, record the high peak temperatures they had immediately after emplacement.

The effect of reducing the total thickness of the intrusions leads to the overall decrease in peak metamorphic temperatures of rocks within the magmatism region. In the model shown in figure 12C, only 6 out of the default configuration of 10 mafic sills were emplaced at mid-crustal depths at 5 Myr. As a result, rocks containing the high-grade K-feldspar-bearing mineral assemblages are diminished in volume and are concentrated in thin zones surrounding the region with peak temperatures exceeding 800 °C (compare with fig. 8D). The volume of rocks that develop minerals in the granulite facies of metamorphism is greatly reduced.

A different sequence of peak metamorphic assemblages is produced when the thickness of individual sills is increased from 500 m to 1000 m (fig. 12D). The total thickness of the intrusion in this model is 3 km, as in the model in figure 12C. However, because a greater volume of magma is emplaced with every individual pulse of magmatism, each intrusion takes longer to cool down below the solidus temperature. The timescale of thermal diffusion of each thermal peak, τ , is increased in proportion to the squared sill thickness, d , according to: $\tau \sim d^2$. Every sill intrusion is therefore recorded in figure 12D with a strip of rocks with $T_p > 800$ °C surrounded by narrow bands of high-T peak metamorphic mineral assemblages that formed in the wall rock as a result of conductive heating. The pressures at which peak temperatures were attained are determined in each case by the depth of the sill emplacement. The sill that is closest to the surface (10 km depth) is sandwiched between the narrow strips of the cordierite-biotite-chlorite and cordierite-biotite-K-feldspar mineral assemblages. As peak temperatures drop with increasing distance from the sill, these mineral assemblages transition to chlorite-biotite on top and staurolite-biotite underneath. The transition from the chlorite-biotite assemblage to cordierite-bearing assemblages occurs over the vertical distance of ~ 1 to 2 km. Deeper sills are surrounded by rocks with higher-P mineral assemblages, such as those from the sillimanite zone. Metamorphic gradients in the lateral direction at the tips of the sills are as steep as in the vertical direction, although the numerical resolution of our models (1 or 2 km in x and 0.5 km in z) does not allow us to reconstruct the details.

Another set of simulations with magmatic sills characterized by a lower emplacement temperature of 850 °C, corresponding to an intermediate-felsic composition, is illustrated in figure 13. The lower emplacement temperature of the magmatic intrusions in the default configuration (10 sills, each 500 m thick) results in a more than 50 °C reduction in the peak metamorphic temperatures in all of the rocks affected by magmatism in comparison to the analogous model with mafic sills (fig. 13A; compare with fig. 8B). The core of the magmatic zone is composed of rocks containing garnet-staurolite-biotite; only a small fraction of rocks surrounding the deepest sills attain temperatures in the kyanite and sillimanite zones (fig. 13C; compare with fig. 8D). For comparison, figures 13B and 13D show the P-T-t paths and the peak metamorphic mineral assemblages for a model with six, 1,000 m thick, intermediate felsic sills emplaced every 200,000 years. The greater volumes of magma emplaced with

each individual intrusion and the correspondingly higher emplacement rate (0.5 cm/yr, instead of 0.25 cm/yr) result in the attainment of higher temperatures and the development of minerals in the sillimanite and sillimanite-K-feldspar zones in the central part of the magmatism region. Interestingly, the resultant distribution of mineral assemblages within the model thrust is very similar to the analogous model with hotter mafic intrusions of 3 km total thickness (that is, 6 sills, each 500 m thick; fig. 12C). This result illustrates the potential non-uniqueness of the model thermal structure in response to the variations in different magmatism parameters. Consequently, assessing the relationships between magmatism and regional metamorphism in specific geologic localities requires that key geologic variables including magma compositions and the volume and spatial dimensions of intrusive bodies be carefully evaluated.

DISCUSSION AND CONCLUSIONS

The results of our numerical modeling, in agreement with previous studies including England and Thompson (1984) and Jamieson and others (1998), demonstrate that peak temperatures during regional metamorphism in tectonically overthickened crust with average crustal and mantle heat production in the absence of magmatism are mostly below 650 to 700 °C at exhumation timescales less than 40 Myr. The attainment of peak metamorphic temperatures due to overthrusting spans at least 5 to 10 Myr (fig. 3A). Higher metamorphic temperatures (in excess of 800 °C) may be reached for longer timescales of exhumation (that is, at lower erosion rates); the thermal peak attainment will then span longer than 10 Myr. In all cases, the high metamorphic temperatures are reached at high pressures at considerable depths within the crustal section (≥ 35 km; fig. 3). The characteristic peak metamorphic mineral assemblages for a representative aluminous pelitic bulk composition therefore include high-temperature high-pressure minerals in the staurolite, kyanite and garnet-biotite (without chlorite) zones.

The introduction of magmatic intrusions into the regional overthrust setting leads to dramatic changes in the thermal structure of the thickened crust. The elevation of peak metamorphic temperatures due to magmatism depends on many factors, such as the timing, temperature and rate of magma emplacement, the depth of emplacement, and the dimensions of individual intrusions. But even for the most conservative sets of parameter values, the peak temperatures in crustal rocks around mafic intrusions are increased by more than 100 °C. The timescales of peak temperature attainment in rocks at short distances from the magmatism region are typically very short, ranging from a few hundred thousand years to about 1 Myr depending on the rate of intrusion (see fig. 4A, B; fig. 7A, B; and fig. 11A, B). The peak temperatures are attained almost synchronously within the different metamorphic zones over a depth range of more than 10 km in the crustal rocks affected by magmatism (see fig. 5A, B and fig. 9A, B).

Magmatic intrusions in our models may produce Buchan and Barrovian-type metamorphic sequences and, if the intrusions are mafic, considerable quantities of rocks in the granulite facies that attain peak temperatures above 800 °C. The specific peak metamorphic mineral assemblages that develop are largely determined by the depth range of magma intrusion. Intrusion into the lower plate of the overthrust zone (35–50 km) leads to significant increases in peak metamorphic temperatures in the entire crustal section, even for rocks that are located at 10 to 20 km below or above the zone of magmatism (figs. 4–6). The peak metamorphic mineral assemblages are very similar to those observed in a model without magmatism: they include minerals in the staurolite, kyanite and the high-pressure, high-temperature garnet-biotite zone (without chlorite) (compare fig. 3 with figs. 4–6). The spatial distributions of the assemblages are, however, very different. Furthermore, considerable volumes of rock within the depth interval of magmatism attain peak temperatures in excess of 800 °C.

Emplacement of magmatic intrusions at mid-crustal depths, on the other hand, may produce very different sequences of mineral assemblages, including those of LP/HT metamorphic zones such as cordierite-biotite-K-feldspar (figs. 7-9, 11). The direct effect of magmatic thermal pulses on the temperature of ambient rocks is more localized than in the case of deep magmatism. Rocks underlying the mid-crustal intrusions, however, are strongly influenced by their displacement towards deeper, hotter parts of the crust. When mid-crustal magmatism is initiated at earlier times in the model thrust exhumation history (less than 15 Myr), the rocks with minerals in LP/HT metamorphic zones may not be preserved in the crustal section due to surface erosion (fig. 7D, 8F).

In all of the models with magmatism, very steep Metamorphic Field Temperature Gradients (MFTGs) are observed around the edges of the intrusions. In some cases, the lateral transition from chlorite to sillimanite zones of metamorphism at the side of the magmatic region may take place over about 1 km (fig. 12A, B). Such strong gradients in peak temperatures, however, are in most cases nearly isobaric. They are produced as a result of strong temperature contrasts between the emplaced magma and the ambient rock, which lead to fast cooling of magmatic intrusions and consequently small length scales of heat transfer by conduction. Steep gradients are also observed along the upper and lower contacts of thick isolated sills (fig. 12D). The steep, magmatism-related MFTGs are very unlike regional metamorphic gradients that appear at the flanks of the overthrust zone, for which the transition from the chlorite zone to high-grade mineral assemblages takes place over 20 to 40 km. The regional MFTGs are not isobaric: the pressure difference from low to high grade may be 0.2 to 0.3 GPa (fig. 3C, D).

An important consequence of these relationships is that rocks within, beneath, and above the region of magmatism have very different P-T-t-X histories than rocks on the flanks of the overthrust zone. Consequently, the flanking rocks cannot be used to infer the progressive P-T-t-X evolution of rocks affected by magmatic heat transfer, including rocks overlying the magmas that have been removed by erosion.

ACKNOWLEDGMENTS

We thank E. F. Baxter, D. M. Rye, and R. S. J. Sparks for thoughtful discussions of metamorphism and magmatism both in the lab and in the field. Critical reviews by S. C. Penniston-Dorland and J. A. D. Connolly greatly improved this paper. The support of the National Science Foundation Directorate for Geosciences (NSF EAR-0509934) is gratefully acknowledged.

APPENDIX

Numerical Model

The model solves the following system of equations for energy conservation (1), mass conservation for fluid (2), and momentum conservation for fluid or Darcy's law (3):

$$\rho_m C_p^m \frac{\partial T}{\partial t} = \nabla \cdot (k_r \nabla T) - C_p^f \nabla \cdot (\mathbf{u}T) - \rho_m C_p^m U \frac{\partial T}{\partial z} + A - \frac{\Delta H_r Q_r}{M_{H_2O}} - \rho_m L \frac{\partial X}{\partial t}, \quad (1)$$

$$\nabla \cdot \mathbf{u} = Q_r - \frac{\partial(\phi\rho)}{\partial t}, \quad (2)$$

$$\mathbf{u} = -\frac{\rho k_\phi}{\mu} (\nabla P_f - \rho \mathbf{g}). \quad (3)$$

The notation and model parameters are summarized in table A1. From left to right, the terms on the right hand side of equation (1) account for heat conduction through the rock mass, fluid advection, exhumation, radiogenic heat production, metamorphic reactions, and crystallization or partial melting, respectively. The

TABLE A1
Notation and typical values used in modeling

| Variable | Value | Unit |
|---------------|---|---|
| A | Radiogenic heat production, surface value | $3 \cdot 10^{-6}$ W m ⁻³ |
| C_p^f | Specific heat of fluid | 1046 J kg ⁻¹ K ⁻¹ |
| C_p^m | Specific heat of the medium (solid + fluid) | 1100 J kg ⁻¹ K ⁻¹ |
| g | Acceleration of gravity | 9.8 m s ⁻² |
| k_c | Thermal conductivity of the medium | 2.25 W m ⁻¹ K ⁻¹ |
| k_ϕ | Permeability | m ² |
| $k_{\phi 0}$ | Reference permeability value | 10^{-19} m ² |
| L | Latent heat of fusion or crystallization in metapelitic rock in igneous rock | $3 \cdot 10^5$ $4 \cdot 10^5$ J kg ⁻¹ K ⁻¹ |
| m_{H_2O} | Molar weight of water | $18 \cdot 10^{-3}$ kg mol ⁻¹ |
| M_{H_2O} | Mass of bound water in metapelitic rocks | wt% |
| n | Porosity-permeability exponent | 2 |
| P | Pressure | Pa |
| P_f | Fluid pressure | Pa |
| q_b | Basal heat flow | $35 \cdot 10^{-3}$ W m ⁻² |
| Q_r | Heat released/consumed by metamorphism | J m ⁻³ |
| t, t | Time | |
| T, T | Temperature | K or °C |
| | Liquidus temperature in metapelite | 1250 °C |
| T_l | in basalt | 1220 °C |
| | in intermediate–felsic magma | 850 °C |
| T_s | Surface temperature | 0 °C |
| | Solidus temperature in metapelitic rock | 725 °C |
| T_{sol} | in basaltic rock | 720 °C |
| | in intermediate–felsic rock | 725 °C |
| u | Fluid flux vector | kg m ⁻² s ⁻¹ |
| U | Rate of erosion | 0.5, 1, 1.5 mm yr ⁻¹ |
| v | Fluid velocity vector | m s ⁻¹ |
| x | Horizontal axis | |
| X | Melt fraction | kg kg ⁻¹ |
| X_f | Fluid release/consumption during metamorphism | 0.045 kg kg ⁻¹ |
| z | Vertical axis, positive downwards | |
| z_A | Length scale of decay of A with depth | 10^4 m |
| ΔH_r | Enthalpy change of metamorphic reaction | J mol ⁻¹ |
| ΔT | Temperature interval for reaction in metapelites | 500 K |
| α | Hydraulic diffusivity | $1.45 \cdot 10^{-3}$ m ² s ⁻¹ |
| β | Fluid compressibility | Pa ⁻¹ |
| μ | Fluid viscosity | $1.15 \cdot 10^{-4}$ Pa s |
| ϕ | Porosity | m ³ m ⁻³ |
| ϕ_0 | Reference porosity | $5 \cdot 10^{-4}$ m ³ m ⁻³ |
| ϕ_{\min} | Minimal porosity | 10^{-6} m ³ m ⁻³ |
| ρ | Fluid density | kg m ⁻³ |
| ρ_m | Density of the medium (rock + fluid) | 2800 kg m ⁻³ |

fluid mass flux u is defined as the product of the fluid density, porosity, and fluid velocity: $u = \rho\phi v$. The energy conservation equation is written with the understanding that the velocity and source/sink terms may all vary with position and time. The above equations are supplemented with the equation of state for the fluid. For simplicity, we assume that metamorphic fluids are composed solely of water. The densities of water over a wide range of pressures and temperatures are calculated using the Compensated-Redlich-Kwong (CORK) equation of state of Holland and Powell (1991, 1998).

The energy conservation equation is solved numerically for each time step using a two-dimensional Alternating Direction Implicit (ADI) method (Ames, 1992). The resultant temperature distribution serves as input to an iterative procedure that solves for internally-consistent fluid pressure, density, and flux distributions using a coupled system of equations formed by mass conservation, momentum conservation, and CORK. If fluid pressure exceeds the threshold for hydrofracturing, then porosity and permeability are increased to simulate hydrofracturing and new solutions for the fluid pressure, density, and fluxes required by the elevated porosity-permeability values are found (Part II). To test the solution procedure, we ran simulations over ranges of time step and grid spacing values and found that the results were consistent over these ranges. Furthermore, the cumulative fluid mass balance error, defined by the unaccounted-for variation in fluid mass in each grid cell divided by the total fluid mass in each cell, is only $\sim 10^{-8}$ kg kg $^{-1}$, indicating excellent conservation of mass by the code (Lyubetskaya and Ague, 2009a).

The initial rock water content (present in hydrous minerals) varies with temperature. Rocks below 400 °C contain 5 weight percent H₂O, whereas the water content of rocks at $T > 400$ °C drops linearly from 5 weight percent to zero over the temperature interval of 300 °C.

We placed the initial “Moho” boundary at the depth where rocks no longer contain structural water bound in hydrous minerals; this corresponds to the 700 °C isotherm (fig. 1). Other choices have no significant impact on our results. In the crust unperturbed by thrusting on the right side of the model, this temperature is reached at a depth of ~ 42 km (model crust thickness ~ 37 km). Thus, in the region of the overthrust, the total thickness of the upper plate (35 km) and the lower plate is about 72 km. This thickness is comparable, for example, to that observed in the modern Himalaya-Tibet orogen (Hirn, 1988).

The metamorphic reaction rate, Q_r , is modeled as a function of the rate of temperature change within a rock parcel (compare Hanson, 1992):

$$Q_r = \frac{X_j \rho_m}{\Delta T} \frac{\partial T}{\partial t} \quad (4)$$

The sign of the temperature change determines the direction in which hydration/dehydration reactions proceed in a particular rock parcel: endothermic dehydration reactions require the addition of heat, whereas exothermic hydration reactions produce it. The rate of prograde reaction is modeled based on a representative value of 4.5 weight percent loss of water in dehydration reactions over the temperature interval of 200 to 700 °C. As discussed in Lyubetskaya and Ague (2009b), reaction is assumed to produce the most water at temperatures between 400 and 650 °C (due largely to reactions involving chlorite breakdown); the average rate of fluid production corresponds to 3 weight percent water loss over 250 °C, or 0.012 weight percent °C $^{-1}$. Average reaction rates for temperatures from 650 to 700 °C and from 200 to 400 °C are 0.01 weight percent °C $^{-1}$ (1 wt% loss) and 0.005 weight percent °C $^{-1}$ (0.5 wt% loss) respectively. Enthalpy changes for metamorphic reactions (ΔH) are modeled as 35 kJ per mole H₂O released for reactions proceeding at $T \leq 420$ °C, and 65 kJ mol $^{-1}$ for higher-T reactions. As ΔH is relatively insensitive to pressure, the above values are used throughout the model crust (see Lyubetskaya and Ague, 2009b, for detailed discussion of rates and enthalpies). Retrogression occurs during cooling. Water is added and reaction is exothermic, but the rates and enthalpies are as described above. Hydration during retrogression is limited to a maximum rock water content of 5 weight percent.

The permeability, k_ϕ , at the surface is held at 10^{-16} m 2 ; k_ϕ decreases with depth exponentially with the characteristic length scale of 2.5 km to the reference background value 10^{-19} m 2 (Lyubetskaya and Ague, 2009a). This value is based on the empirical integrated estimate of permeability for the middle and deep crust proposed by Manning and Ingebritsen (1999). We note that permeability estimates for the upper crust can be obtained in a number of ways including *in-situ* measurement in boreholes and regional groundwater/thermal modeling (Manning and Ingebritsen, 1999, and references therein). They are arguably better constrained than those for deeper metamorphic rocks, which rely on petrologic estimates of time-integrated fluid fluxes. At high temperatures, permeability in our models decreases exponentially with increasing temperature, from 10^{-19} at 700 °C to $\sim 10^{-21}$ m 2 at 900 °C. The reference porosity for the flow region, ϕ_0 , is set to the representative value of $5 \cdot 10^{-4}$ (compare Connolly, 1997; Hiraga and others, 2001). Feedbacks

between porosity and permeability are only considered for hydrofracturing (Part II); in addition, some aspects of reaction-induced feedbacks are discussed by Lyubetskaya and Ague (2009a).

The initial fluid pressure gradient is defined by the hydrostat, and is continuous across the model thrust. We assume that any “sawtooth” gradient related to thrusting is removed in the first 0.5 million years of model time (the timescale over which the geotherm is allowed to relax before intrusion and metamorphism begin; see text). The hydraulic diffusivity, α , provides a rough indicator of how rapidly a fluid pressure heterogeneity will relax with time: $\alpha = k_{\phi 0} / (\phi_0 \beta \mu)$ (Bear, 1988; Talwani and Acree, 1984). Here, $k_{\phi 0}$ is the permeability (10^{-19} m^2), ϕ_0 is the porosity ($5 \cdot 10^{-4}$), μ is the fluid viscosity ($1.15 \cdot 10^{-4} \text{ Pa s}$), and β is the isothermal fluid compressibility. Compressibility is small at the P-T conditions of interest and decreases with pressure; for example, it is $1.2 \cdot 10^{-9} \text{ Pa}^{-1}$ at 600 °C and 0.3 GPa, and $2.4 \cdot 10^{-10} \text{ Pa}^{-1}$ at 600 °C and 1.0 GPa (CORK equation of state). Using a generous compressibility of $1.2 \cdot 10^{-9} \text{ Pa}^{-1}$ and the representative values for other parameters given above yields $\alpha = 1.45 \cdot 10^{-3} \text{ m}^2 \text{ s}^{-1}$. This value is ~ 2000 times larger than the thermal diffusivity, indicating that any sawtooth fluid pressure gradient would be short-lived. For example, if we define the characteristic length scale l for fluid pressure relaxation as $l = \sqrt{\alpha \cdot t}$, then l exceeds 20 km even for timescales as short as 10^4 years.

Several important initial and boundary conditions for model fluid flow are shown in figure 1. The upper surface of the model is held at constant atmospheric pressure. No flow is allowed across the left boundary at $x = 0$ km or the right boundary at $x = 240$ km by imposing a “no-flux” (or “symmetrical”) boundary condition: $\partial P_f / \partial x = 0$ for all model times t . As a result, the component of the fluid mass flux in the x direction, u_x , is zero according to Darcy’s law (eq. 3). The base of the flow model corresponds to the 900 °C isotherm in the mantle. It moves upward with time in the overthrust region as a result of exhumation. A vertical hydrostatic pressure gradient is imposed along this boundary: $\partial P_f / \partial z = \rho g$ (g , the acceleration of gravity, is treated here as a constant). Consequently, the vertical velocity of flow, v_z , is zero, and there is no fluid flux that can move upward from this boundary into the crustal section. Furthermore, in the region where the boundary slopes ($x = 60\text{--}120$ km), the condition $\partial P_f / \partial x = 0$ is employed such that no flow occurs in the horizontal direction either. Note as well that rock below the model “Moho”: 1) has exponentially-decreasing permeability and 2) contains no hydrous minerals and therefore does not produce fluid via devolatilization reactions. We emphasize that we are not attempting to model fluid transport in the mantle. Instead, our goal is simply to provide appropriate initial and boundary conditions so that the model mantle is not a source of fluid flow into the crust.

The initial thermal structure is calculated based on a steady-state crustal geotherm (Turcotte and Schubert, 2002):

$$T = T_s + \frac{q_b z}{k_c} + \frac{A z_A^2}{k_c} (1 - e^{-z/z_A}). \quad (5)$$

The concentration of radiogenic heat-producing elements in the crust is assumed to decay exponentially with depth with the characteristic length scale z_A equal 10 km. The surface value of radiogenic heat production $A = 3 \cdot 10^{-6} \text{ W m}^{-3}$ (Hanson, 1997), and the basal heat flow $q_b = 35 \cdot 10^{-3} \text{ W m}^{-2}$ (see Lyubetskaya and Ague, 2009a, for additional discussion). These values yield a surface heat flow of $\sim 60 \cdot 10^{-3} \text{ W m}^{-2}$ (Jaupart and Mareschal, 2003). Thrusting results in an initial sawtooth radiogenic heat production profile. The right boundary of the model at $x = 240$ km is maintained at the steady-state temperature distribution over the entire simulation time (fig. 1). The left boundary at $x = 0$ km is a no-flux boundary that does not transfer heat in the horizontal dimension. Consequently, at this boundary, $F_x = 0 = -k_c (\partial T / \partial x) + C_p u_x T$, where F_x is the heat flux in the x direction. As noted above, the fluid flow boundary condition sets $u_x = 0$; the conductive flux is set to zero by prescribing $\partial T / \partial x = 0$. The surface has a constant temperature $T_s = 0$ °C.

The partial melting curve for metapelitic rocks in Annen and others (2006) specifies that the melt fraction increases as a step function from 0 to 0.06 at the solidus temperature of 725 °C. To decrease spurious temperature oscillations and increase numerical stability, the curve was modified slightly to increase from 0 to 0.06 over the temperature interval 715 to 725 °C.

REFERENCES

- Ague, J. J., and Baxter, E. F., 2007, Brief thermal pulses during mountain building recorded by Sr diffusion in apatite and multicomponent in garnet: *Earth and Planetary Science Letters*, v. 261, p. 500–516, doi: 10.1016/j.epsl.2007.07.017.
- Ames, W. F., 1992, *Numerical methods for partial differential equations*, 3rd edition: San Diego, Academic Press, Inc., 451 p.

- Annen, C., and Sparks, R. S. J., 2002, Effects of repetitive emplacement of basaltic intrusions on thermal evolution and melt generation in the crust: *Earth and Planetary Science Letters*, v. 203, p. 937–955, doi: 10.1016/S0012-821X(02)00929-9.
- Annen, C., Blundy, J. D., and Sparks, R. S. J., 2006, The genesis of intermediate and silicic magmas in deep crustal hot zones: *Journal of Petrology*, v. 47, p. 505–539, doi: 10.1093/petrology/egi084.
- Barrow, G., 1893, On an intrusion of muscovite-biotite gneiss in the south-eastern Highlands of Scotland, and its accompanying metamorphism: *Geological Society of London Quarterly Journal*, v. 49, p. 330–358, doi: 10.1144/GSL.JGS.1893.049.01-04.52.
- Barton, M. D., and Hanson, R. B., 1989, Magmatism and the development of low-pressure metamorphic belts: Implications from the western United States and thermal modeling: *Geologic Society of America Bulletin*, v. 101, p. 1051–1065, doi: 10.1130/0016-7606(1989)101<1051:MATDOL>2.3.CO;2.
- Baxter, E. F., Ague, J. J., and DePaolo, D. J., 2002, Prograde temperature-time evolution in the Barrovian type-locality constrained by Sm/Nd garnet ages from Glen Clova, Scotland: *Journal of the Geologic Society, London*, v. 159, p. 71–82, doi: 10.1144/0016-76901013.
- Bear, J., 1988, *Dynamics of fluids in porous media*: New York, Dover, 764 p.
- Bernet, M., Massimiliano, Z., Garver, J. I., Brandon, M. T., and Vance, J. A., 2001, Steady-state exhumation of the European Alps: *Geology*, v. 29, p. 35–38, doi: 10.1130/0091-7613(2001)029<0035:SSEOTE>2.0.CO;2.
- Brady, J. B., 1988, The role of volatiles in the thermal history of metamorphic terranes: *Journal of Petrology*, v. 29, p. 1187–1213, doi: 1187-1213; doi: 10.1093/petrology/29.6.1187.
- Brandon, M. T., Roden-Tice, M. K., and Garver, J. I., 1998, Late Cenozoic exhumation of the Cascadia accretionary wedge in the Olympic Mountains, northwest Washington State: *Geological Society of America Bulletin*, v. 110, p. 985–1009, doi: 10.1130/0016-7606(1998)110<0985:LCEOTC>2.3.CO;2.
- Bucholz, C. E., and Ague, J. J., 2009, Fluid flow and Al transport during quartz-kyanite vein formation, Unst, Shetland Islands, Scotland: *Journal of Metamorphic Geology*, v. 28, p. 19–39, doi: 10.1111/j.1525-1314.2009.00851.x.
- de Capitani, C., 1994, Gleichgewichts-Phasendiagramme: Theorie und Software: Beihefte zum *European Journal of Mineralogy*, 72. Jahrestagung der Deutschen Mineralogischen Gesellschaft, 6, 48.
- de Capitani, C., and Brown, T. H., 1987, The computation of chemical equilibrium in complex systems containing non-ideal solutions: *Geochimica et Cosmochimica Acta*, v. 51, p. 2639–2652, doi: 10.1016/0016-7037(87)90145-1.
- Connolly, J. A. D., 1997, Devolatilization-generated fluid pressure and deformation-propagated fluid flow during prograde regional metamorphism: *Journal of Geophysical Research*, v. 102, n. B8, p. 18149–18173, doi: 10.1029/97JB00731.
- Crisp, J., 1984, Rates of magma emplacement and volcanic output: *Journal of Volcanology and Geothermal Research*, v. 20, p. 177–211, doi: 10.1016/0377-0273(84)90039-8.
- De Yoreo, J. J., Lux, D. R., and Guldotti, C. V., 1991, Thermal modelling in low-pressure/high-temperature metamorphic belts: *Tectonophysics*, v. 188, p. 209–238, doi: 10.1016/0040-1951(91)90457-4.
- Dorais, M. J., 2003, The petrogenesis and emplacement of the New Hampshire plutonic suite: *American Journal of Science*, v. 303, p. 447–487, doi: 10.2475/ajs.303.5.447.
- Dutrow, B. L., Foster, C. T., Gable, C., and Travis, B., 2010, Time-dependent 3-D modeling of contact-regional metamorphism suggests reactions occur in <1 Ma: Knoxville, Tennessee, June 13–18, 20th Annual Goldschmidt Conference, Goldschmidt Conference Abstracts, p. A. 254.
- England, P. C., and Thompson, A. B., 1984, Pressure-temperature-time paths of regional metamorphism. I. Heat transfer during the evolution of regions of thickened continental crust: *Journal of Petrology*, v. 25, p. 894–928, doi: 10.1093/petrology/25.4.894.
- Fitzgerald, P. G., Stump, E., and Redfield, T. F., 1993, Late Cenozoic uplift of Denali and its relation to relative plate motion and fault morphology: *Science*, v. 259, p. 497–499, doi: 10.1126/science.259.5094.497.
- Friedrich, A. M., Bowring, S. A., Martin, M. W., and Hodges, K. V., 1999, Short-lived continental magmatic arc at Connemara, western Irish Caledonides: implications for the age of the Grampian orogeny: *Geology*, v. 27, p. 27–30, doi: 10.1130/0091-7613(1999)027<0027:SLCMAA>2.3.CO;2.
- Gerya, T. V., Perchuk, L. L., Maresch, W. V., Willner, A. P., Van Reenen, D. D., and Smit, C. A., 2002, Thermal regime and gravitational instability of multi-layered continental crust: implications for the buoyant exhumation of high-grade metamorphic rocks: *European Journal of Mineralogy*, v. 14, p. 687–699, doi: 10.1127/0935-1221/2002/0014-0687.
- Gorring, M. L., and Kay, S. M., 2001, Mantle processes and sources of Neogene slab window magmas from southern Patagonia, Argentina: *Journal of Petrology*, v. 42, p. 1067–1094, doi: 10.1093/petrology/42.6.1067.
- Hanson, R. B., 1992, Effects of fluid production on fluid flow during regional and contact metamorphism: *Journal of Metamorphic Geology*, v. 10, p. 87–97, doi: 10.1111/j.1525-1314.1992.tb00073.x.
- 1997, Hydrodynamics of regional metamorphism due to continental collision: *Economic Geology*, v. 92, p. 880–891, doi: 10.2113/gsecongeo.92.7-8.880.
- Hanson, R. B., and Barton, M. D., 1989, Thermal development of low-pressure metamorphic belts: Results from two-dimensional numerical models: *Journal of Geophysical Research*, v. 94, n. B8, p. 10363–10377, doi: 10.1029/JB094iB08p10363.
- Hiraga, T., Osamu, N., Nagase, T., and Akizuki, M., 2001, Morphology of intergranular pores and wetting angles in pelitic schists studied by transmission electron microscopy: *Contributions to Mineralogy and Petrology*, v. 141, p. 613–622, doi: 10.1007/s004100100263.
- Hirn, A., 1988, Features of the crust-mantle structure of the Himalayas-Tibet: a comparison with seismic traverses of Alpine, Pyrenean and Variscan orogenic belts: *Philosophical Transactions of the Royal Society of London, Series A*, v. 326, p. 17–32.

- Holland, T., and Powell, R., 1991, A Compensated-Redlich-Kwong (CORK) equation for volumes and fugacities of CO₂ and H₂O in the range 1 bar to 50 kbar and 100–1600 °C: *Contributions to Mineralogy and Petrology*, v. 109, p. 265–273, doi: 10.1007/BF00306484.
- 1998, An internally consistent thermodynamic data set for phases of petrological interest: *Journal of Metamorphic Geology*, v. 16, p. 309–343, doi: 10.1111/j.1525-1314.1998.00140.x.
- Huerta, A. D., Royden, L. H., and Hodges, K. V., 1996, The interdependence of deformational and thermal processes in mountain belts: *Science*, v. 273, p. 637–639, doi: 10.1126/science.273.5275.637.
- Jamieson, R. A., Beaumont, C., Fullsack, P., and Lee, B., 1998, Barrovian regional metamorphism: where's the heat?, *in* Treolar, P. J., and O'Brien, P. J., editors, *What Drives Metamorphism and Metamorphic Reactions?*: Geological Society, London, Special Publications, v. 138, p. 23–51, doi: 10.1144/GSL.SP.1996.138.01.03.
- Jaupart, C., and Mareschal, J.-C., 2003, Constraints on crustal heat production from heat flow data, *in* Rudnick, R. L., editor, *The Crust: Treatise on Geochemistry*, v. 3, p. 65–84, doi: 10.1016/B0-08-043751-6/03017-6.
- Jónsson, S., Zebker, H., and Amelung, F., 2005, On trapdoor faulting at Sierra Negra volcano, Galápagos: *Journal of Volcanology and Geothermal Research*, v. 144, p. 59–71, doi: 10.1016/j.jvolgeores.2004.11.029.
- Lancaster, P. J., Baxter, E. F., Ague, J. J., Breeding, C. M., and Owens, T. L., 2008, Synchronous peak Barrovian metamorphism driven by syn-orogenic magmatism and fluid flow in southern Connecticut, USA: *Journal of Metamorphic Geology*, v. 26, p. 527–538, doi: 10.1111/j.1525-1314.2008.00773.x.
- Lux, D. R., De Yoreo, J. J., Guldotti, C. V., and Decker, E. R., 1986, Role of plutonism in low-pressure metamorphic belt formation: *Nature*, v. 323, p. 794–797, doi: 10.1038/323794a0.
- Lyubetskaya, T., and Ague, J. J., 2009a, Modeling the magnitudes and directions of regional metamorphic fluid flow in collisional orogens: *Journal of Petrology*, v. 50, p. 1505–1531, doi: 10.1093/petrology/egp039.
- 2009b, Effects of metamorphic reaction on thermal evolution in collisional orogens: *Journal of Metamorphic Geology*, v. 27, p. 579–600, doi: 10.1111/j.1525-1314.2009.00847.x.
- Mahon, K. L., Harrison, T. M., and Drew, D. A., 1988, Ascent of a granulite diapir in a temperature-varying medium: *Journal of Geophysical Research*, v. 93, p. 1174–1188, doi: 10.1029/JB093iB02p01174.
- Manning, C. E., and Ingebritsen, S. E., 1999, Permeability of the continental crust: implications of geothermal data and metamorphic systems: *Reviews of Geophysics*, v. 37, p. 127–150, doi: 10.1029/1998RG900002.
- Marsh, B. D., 1982, On the mechanics of igneous diapirism, stoping and zone melting: *American Journal of Science*, v. 282, p. 808–855.
- Miyashiro, A., 1973, *Metamorphism and metamorphic belts*: London, George Allen and Unwin, 492 p.
- Moore, M. A., and England, P. C., 2001, On the inference of denudation rates from cooling ages of minerals: *Earth and Planetary Science Letters*, v. 185, p. 265–284, doi: 10.1016/S0012-821X(00)00380-0.
- Oliver, G. J. H., Wilde, S. A., and Wan, Y., 2008, Geochronology and geodynamics of Scottish granulites from the late Neoproterozoic break-up of Rodinia to Palaeozoic collision: *Journal of the Geological Society, London*, v. 165, p. 661–674, doi: 10.1144/0016-76492007-105.
- Powell, R., Holland, T., and Worley, B., 1998, Calculating phase diagrams involving solid solutions via non-linear equations, with examples using THERMOCALC: *Journal of Metamorphic Geology*, v. 16, p. 577–588, doi: 10.1111/j.1525-1314.1998.00157.x.
- Reverdatto, V. V., and Polyansky, O. P., 2004, Modelling of the thermal history of metamorphic zoning in the Connemara region (western Ireland): *Tectonophysics*, v. 379, p. 77–91, doi: 10.1016/j.tecto.2003.10.005.
- Safran, E. B., Blythe, A., and Dunne, T., 2006, Spatially variable exhumation rates in orogenic belts: an Andean example: *Journal of Geology*, v. 114, p. 665–681, doi: 10.1086/507613.
- Shi, Y., and Wang, C.-Y., 1987, Two-dimensional modeling of the *P-T-t* paths of regional metamorphism in simple overthrust terrains: *Geology*, v. 15, p. 1048–1051, doi: 10.1130/0091-7613(1987)15<1048:TMOTPP>2.0.CO;2.
- Sisson, V. B., Hollister, L. S., and Onstott, T. C., 1989, Petrologic and age constraints on the origin of a low-pressure/high-temperature metamorphic complex, southern Alaska: *Journal of Geophysical Research*, v. 94, p. 4392–4410, doi: 10.1029/JB094iB04p04392.
- Talwani, P., and Acree, S., 1984, Pore pressure diffusion and the mechanism of reservoir-induced seismicity: *Pure and Applied Geophysics*, v. 122, p. 947–965, doi: 10.1007/BF00876395.
- Turcotte, D. L., and Schubert, G., 2002, *Geodynamics: Applications of continuum physics to geological problems*: New York, John Wiley & Sons, 456 p.
- Vielzeuf, D., and Holloway, J. R., 1988, Experimental determination of the fluid-absent melting relations in the pelitic system: *Contributions to Mineralogy and Petrology*, v. 98, p. 257–276, doi: 10.1007/BF00375178.
- Whittington, A. G., Hofmeister, A. M., and Nabelek, P. I., 2009, Temperature-dependent thermal diffusivity of the Earth's crust and implications for magmatism: *Nature*, v. 458, p. 319–321, doi: 10.1038/nature07818.
- Wickham, S. M., and Oxburgh, E. R., 1985, Continental rifts as a setting for regional metamorphism: *Nature*, v. 318, p. 330–333, doi: 10.1038/318330a0.
- Willett, S. D., and Brandon, M. T., 2002, On steady states in mountain belts: *Geology*, v. 30, p. 175–178, doi: 10.1130/0091-7613(2002)030<0175:OSSIMB>2.0.CO;2.
- Willett, S. D., Fisher, D., Fuller, C., Yeh, E.-C., and Lu, C.-Y., 2003, Erosion rates and orogenic-wedge kinematics in Taiwan inferred from fission track thermochronometry: *Geology*, v. 31, p. 945–948, doi: 10.1130/G19702.1.
- Yardley, B. W. D., Barber, J. P., and Gray, J. R., 1987, The metamorphism of the Dalradian rocks of western Ireland and its relation to tectonic setting: *Philosophical Transactions of the Royal Society of London, Series A*, v. 321, p. 243–270.